An iterative algorithm to simultaneously retrieve aerosol extinction and effective radius profiles using the CALIOP lidar

Liang Chang[1], Jing Li[1, 2#], Jingjing Ren [32], Changrui Xiong[1], Lu Zhang [43,54]

[1] *Department of Atmospheric and Oceanic Sciences, School of Physics, Peking University, Beijing 100871, China*

[2]*Collaborative Innovation Center on Forecast and Evaluation of Meteorological Disasters (CIC-FEMD), Nanjing University of Information Science & Technology, Nanjing, 210044, China*

[32] *Intelligent Science & Technology Academy Limited of CASIC*

[43] *Key Laboratory of Radiometric Calibration and Validation for Environmental Satellites, National Satellite Meteorological Center (National Center for Space Weather), China Meteorological Administration, Beijing 100081, China*

[54] *Innovation Center for FengYun Meteorological Satellite (FYSIC), Beijing 100081, China*

 # Correspondence to: Jing Li (jing-li@pku.edu.cn)

Abstract

The Cloud-Aerosol Lidar with Orthogonal Polarization (CALIOP) onboard the Cloud-Aerosol Lidar and Infrared Pathfinder Satellite Observation (CALIPSO) satellite has been widely used in climate and environment studies to obtain the vertical profiles of atmospheric aerosols. To retrieve the vertical profile of aerosol extinction, the CALIOP algorithm assumes column-averaged lidar ratios based on a clustering of aerosol optical properties measured at surface stations. On one hand, these lidar ratio assumptions may not be appropriate or representative at certain locations. One the other hand, the two-wavelength design of CALIOP has the potential to constrain aerosol size information, which has not been considered in the operational algorithm. In this study, we present a modified inversion algorithm to simultaneously retrieve aerosol extinction and effective radius profiles using two-wavelength elastic lidars such as the CALIOP.

Specifically, a look-up table is built to relate the lidar ratio with the Ångström exponent calculated using aerosol extinction at the two wavelengths, and the lidar ratio is then determined iteratively without a priori assumption. The retrieved two-wavelength extinction at each layer is then converted to particle effective radius assuming a lognormal distribution. The algorithm is tested on synthetic data, Raman lidar measurements and then finally the real CALIOP backscatter measurements. Results show improvements over the CALIPSO operational algorithm by comparing with ground-based Raman lidar profiles.

1 Introduction

Atmospheric aerosols have important impacts on the physical and chemical processes in atmosphere, as well as the climate system and public health. Optical properties of aerosols are critical in quantifying their radiative effects in the Earth's climate system. Moreover, the vertical distribution of aerosol properties, such as its extinction coefficient and particle size, is one of the key elements to assess climate effect ~~(Ipcc, 2023)~~(IPCC, 2023). Direct aerosol radiative forcing, which plays an important role in the Earth's energy budget, is impacted by the vertical distribution of aerosols, especially that for absorbing aerosols ~~(Goto et al., 2011; Eswaran et al., 2019; Zhang et al., 2022)~~(Goto et al., 2011; Eswaran et al., 2019; Zhang et al., 2022). The vertical profiles of aerosol optical properties is also essential estimating the solar heating rate ~~(Kudo et al., 2016)~~(Kudo et al., 2016), and establishment of aerosol parameterization schemes for satellite remote sensing ~~(He et al., 2016)~~(He et al., 2016). Although its importance is widely recognized, aerosol vertical distribution is very difficult to monitor globally. Lidar is a major technique for obtaining the profiles of the aerosol properties, which has been used in ground-based and satellite remote sensing systems. Especially, spaceborne lidar is an effective way to observe the global distribution of aerosols. The Cloud-Aerosol Lidar with Orthogonal Polarization (CALIOP) on the CALIPSO (The Cloud-Aerosol Lidar and Infrared Pathfinder Satellite Observation) satellite, the only long-term orbiting spaceborne lidar to date, was launched on 28 April 2006. The CALIOP is a three-channel Mie-scattering lidar system, which contains two wavelengths of ~~532*nm*~~532 nm (perpendicular & parallel polarization channel) and ~~1064*nm*~~1064 nm. It is the first

polarization lidar to provide three-channel elastic backscatter signals of global atmospheric measurements. The official aerosol retrieval algorithm of CALIOP involves three modules, namely the Selective Iterated BoundarY Locator (SIBYL), the Scene Classification Algorithm (SCA), and the Hybrid Extinction Retrieval Algorithms (HERA). The HERA algorithm requires a lidar ratio (extinction-to-backscatter ratio of aerosols), which is provided by the SCA. The SCA uses three CALIOP channels (~~532*nm*~~532 nm parallel, ~~532*nm*~~532 nm perpendicular and ~~1064*nm*~~1064 nm channels) to obtain the lidar ratio from the 6 groups of assumed column-averaged lidar ratios based on a clustering of aerosol optical properties measured at surface stations ~~(Winker et al., 2009)~~(Winker et al., 2009)~~. However, due to the limited coverage and spatial representativeness of surface stations, these lidar ratio assumptions may not be appropriate or representative at certain locations (Josset et al., 2011), which is an important source of retrieval uncertainty.~~.

The lidar ratio is dependent on the chemical composition, shape, particle size distribution of aerosols, as well as the lidar wavelength (Burton et al., 2012), which is a critical parameter required for solving the Mie-scattering lidar equation using the Klett ~~(Klett, 1985)~~(Klett, 1985) or Fernald ~~(Fernald, 1984)~~(Fernald, 1984) methods. Previous studies have developed algorithms to determine the lidar ratio iteratively for two-wavelength Mie scattering lidars. ~~Potter (1987)~~Potter (1987) first introduced the two-wavelength lidar inversion technique to retrieve the aerosol transmission with a constant lidar ratio in two independent wavelengths. Ackermann (Ackermann, 1997, 1998) developed an iterative method to obtain the variable lidar ratio from two-component (i.e., molecule and aerosol) atmospheres by transcendental equation. ~~Rajeev and Parameswaran (1998)~~Rajeev and Parameswaran (1998) proposed a new method using the Mie theory calculated aerosol optical properties with Junge distribution of aerosols to determine the lidar ratio by iteration. ~~Lu et al. (2011)~~Lu et al. (2011) made an attempt to improve the two-wavelength lidar inversion by iterative method, but failed to consider the size distribution of aerosols which may introduce uncertainties in the inversion. Moreover, these studies mostly only gave the aerosol extinction profile without retrieving the vertical distribution of aerosol size information. The algorithms were also mostly applied to theoretical data

or ground lidar measurements. The application to space lidars such as CALIOP is challenging and thus limited.

In view of the above discussions, this study aims to provide a modified two-wavelength lidar inversion algorithm to retrieve the vertical distribution of both aerosol extinction and particle effective radius, avoiding the complex calculation confronted in the previous two-wavelength lidar inversion methods. The algorithm is tested on synthetic data, surface Raman lidar and is finally applied to CALIOP measurements, in order to better demonstrate its operational feasibility. The paper proceeds with descriptions of the inversion algorithm in Sect. 2. Sect. 3 presents the application of the algorithm to the Raman lidar and CALIOP with an analysis of retrieval uncertainties provided in Sect. 4. The study concludes in Sect. 5 with a brief discussion in the context of relevant lidar algorithms.

2 Description of the lidar inversion algorithm

The modified inversion algorithm retrieves the profiles of aerosol extinction and effective radius at two wavelengths, by solving the lidar equation using the Fernald method ~~(Fernald, 1984)~~(Fernald, 1984) with a look-up table approach in the iteration procedure.

2.1 Solving the lidar equation

For each wavelength with a complete overlap between the fields of view of the laser and of the receiver, the lidar equation with calibration and range-correction can be expressed as:

$$\beta'(R) = \frac{P(R)R^2}{E_0\xi} = \left[\beta_m(R) + \beta_p(R)\right]T_m^2(R)T_p^2(R), \quad (1)$$

where

$$T^2(R) = e^{-2\tau(R)}, \quad (2)$$

$$\tau(R) = \int_{R_0}^{R} \sigma(r)dr, \quad (3)$$

In Eq. (1-3) , $\beta'(R)$ is the attenuated backscatter coefficients (calibrated and range-corrected signal) from distance R; $P(R)$ is the measured signal after background subtraction and artefact removal from

distance R; E_0 is the average laser energy for the single-shot; ξ is the lidar system parameter; $\beta(R)$ and $\sigma(R)$ are the volume backscatter and extinction coefficient at range R, respectively; $T^2(R)$ is the ~~one~~two-way transmittance from the lidar to the scattering volume at range R; $\tau(R)$ is the optical depth at range R; and the subscripts M and P denote the portions of air molecules and aerosols, respectively.

In order to facilitate calculation, the transmittance of air molecules $T_m^2(R)$ is separated from $\beta'(R)$ to obtain the $E(R)$ as

$$E(R) = \frac{\beta'(R)}{T_m^2(R)}, \quad (4)$$

As is well known, lidar back scatter signal is also subject to multiple scattering effects. These effects are typically small for low to moderate aerosol loading, and is only significant for optically thick clouds ~~[7].~~ (Winker et al., 2009). Therefore, we neglect multiple scattering effects here and consider that the lidar ratio ($S(R)$) of aerosols is range dependent in single-scatter approximation, which can be written as

$$S(R) = \frac{\sigma_p(R)}{\beta_p(R)}, \quad (5)$$

In the following, we use the Fernald method (Ackermann, 1998) to obtain the aerosol extinction coefficient at distance R as

$$\sigma_p(R) = S(R)\left\{E(R)e^{-2\int_{R_0}^{R} S(r)\beta_m(r)dr}\left[C - 2\int_{R_0}^{R} E(r)S(r)e^{-2\int_{R_0}^{r} S(r')\beta_m(r')dr'}dr\right)\right]^{-1} - \beta_m(R)\Bigg\}, \quad (6)$$

where

$$C = \frac{\beta'(R_0)}{\beta_p(R_0)+\beta_m(R_0)}, \quad (7)$$

The backscatter and extinction coefficient of air molecules can be determined with the Rayleigh scattering theory with the observed atmospheric profile (Bodhaine et al., 1999) as

$$\sigma_m(R,\lambda) = \frac{C_s(\lambda)P(R)}{T(R)}, \quad (8)$$

$$\beta_m(R,\lambda) = \frac{\sigma_m(R,\lambda)}{\frac{8\pi}{3}k_{b\omega}(\lambda)}, \quad (9)$$

Where $P(R)$ and $T(R)$ are the atmospheric pressure (hPa) and temperature (K) at distance R, respectively. $C_s(\lambda)$ and $k_{b\omega}(\lambda)$ are the atmospheric molecular constant related to the wavelength λ. ~~Hostetler et al. (2006) suggested the values of $C_s(\lambda)$ and $k_{b\omega}(\lambda)$ at $532nm$ and $1064nm$ as $C_s(532nm) = 3.742 \times 10^{-6}(K/hPa/m)$; $C_s(1064nm) = 2.265 \times 10^{-7}(K/hPa/m)$; $k_{b\omega}(532nm) = 1.0313$; $k_{b\omega}(1064nm)$~~Hostetler et al. (2006) suggested the values of $C_s(\lambda)$ and $k_{b\omega}(\lambda)$ at $532\ nm$ and $1064\ nm$ as $C_s(532\text{ nm}) = 3.742 \times 10^{-6}$ (K/hPa/m); $C_s(1064\ nm) = 2.265 \times 10^{-7}$ (K/hPa/m); $k_{b\omega}(532\text{ nm}) = 1.0313$; $k_{b\omega}(1604\text{ nm}) = 1.0302$.

Thus, the aerosol extinction coefficient profiles can be obtained by Eq. (6) with an unknown variable of the lidar ratio. The two-wavelength lidar can give two independent profiles of attenuated backscatter coefficients at different wavelengths, from which the aerosol extinction coefficient profiles can be calculated by assuming the lidar ratios at the two wavelengths.

For two wavelengths (λ_1& λ_2), the Ångström exponent (AE) at distance R is defined as:

$$AE(R) = -\frac{ln\left[\frac{\sigma_P(R,\ \lambda_1)}{\sigma_P(R,\ \lambda_2)}\right]}{ln\left[\frac{\lambda_1}{\lambda_2}\right]}, \quad (10)$$

Because *AE* is related to particle effective radius, which is a primary factor determining the lidar ratio, an *AE*-lidar ratio relationship can be established and used to determine the lidar ratio at each layer, which can then be used to retrieve aerosol extinction profiles from two-wavelength lidar measurements.

2.2 Look-up table

By assuming spherical particles ~~with some~~ size distribution, the aerosol extinction coefficients and backscatter coefficients can be calculated by Eq. (11-12):

$$\sigma_p(\lambda) = \int_{r_{min}}^{r_{max}} Q_e(\lambda, r)\, \pi r^2 n(r) dr, \quad (11)$$

$$\beta_p(\lambda) = \int_{r_{min}}^{r_{max}} Q_b(\lambda, r)\, \pi r^2 n(r) dr, \quad (12)$$

Where $n(\mathrm{r})$ represents the volume-size distribution of particles; r_{max} and r_{min} are the maximum and minimum of the particle effective radius, respectively; $Q_e(\lambda, r)$ and $Q_b(\lambda, r)$ denote the extinction ~~efficiency~~

and backscatter factor of the particle with size r at wavelength λ. The size parameter is defined as $x \equiv 2\pi r / \lambda$, where $1 < x < 50$ for typical aerosols and thus the Mie scattering theoryand backscatter efficiency of the particle (the scatter factor of the particle at 180°) with size r at wavelength λ respectively. The size parameter is defined as $x \equiv 2\pi r / \lambda$, where $1 < x < 50$ for typical aerosols and thus the Mie scattering theory (Mishchenko and Yang, 2018) can be applied.

As the limited information provided by two-wavelength lidar, we assume the volume-size distribution of aerosols conform to the lognormal distribution, and the size distribution is expressed as follows: (Deshler et al., 2003; Hara et al., 2021):

$$n(r) = \frac{N}{\sqrt{2\pi}s_d} e^{-\frac{(r-\bar{r})^2}{2s_d^2}}, \quad (13)$$

$$n(r) = \frac{N}{r \ln s_d \sqrt{2\pi}} e^{-\frac{(\ln r - \ln r_0)^2}{2(\ln s_d)^2}}, \quad (13)$$

Where N is the total particle concentration; $\bar{r}$ is concentrations; r_0 and s_d are the average particle median radius; s_d is and the geometric standard deviation. of aerosol size distribution, respectively. When the s_d isswe assumed a constant ins_d for the same aerosol type, the AE can be determinedcalculated with a given r_0 value. The particle effective radius ($\bar{r}$) is defined by the r.:

$$\bar{r} = \frac{\sum n(r) r^3}{\sum n(r) r^2}, \quad (14)$$

We choose the six types of aerosols with their parameters in Table 1, which is consistent with the aerosol classification used in the operational algorithm of CALIOP. (Winker et al., 2009). From Table 1, Type 3 denotes the scattering aerosols, Type 2 shows both strong scattering and absorption, whereas other types are moderate scattering or absorbing. Combining Eqs. (5, 10-1314), the relationship between Ångström exponent (AE) and lidar ratio (S), as well as that between AE and particle effective radius (r)$\bar{r}$) can be formulated as look-up tables for different refractive indices, as shown in Figure 1. Note that in Figure 1, it is easy to determine S_{532nm}, $S_{1064nm}$$S_{532\,nm}$, $S_{1064\,nm}$ and $\bar{r}$ by the unique AE calculated from the lidar equation for a fixed aerosol type.

2.3 The iterative inversion procedure

After constructing the look-up table, we design the following iterative procedure to simultaneously retrieve aerosol extinction and effective radius profiles. Firstly, we calculate the extinction coefficients ($\sigma_{532nm}\sigma_{532\,nm}$ & $\sigma_{1064nm}\sigma_{1064\,nm}$) of two wavelengths ($532nm$ & $1064nm532\ nm$ & $1064\ nm$) from an initial guess of the lidar ratios ($S^0_{532nm}S^0_{532\,nm}$ & $S^0_{1064nm}S^0_{1064\,nm}$) by solving the lidar equation (Eq. 6), then obtain the Ångström exponent (AE) through Eq. (10). Secondly, the look-up table are used to determine a set of new lidar ratios ($S'_{532nm}S'_{532\,nm}$ & $S'_{1064nm}S'_{1064\,nm}$), which is used to calculate the new $\sigma_{532nm}\sigma_{532\,nm}$ & $\sigma_{1064nm}\sigma_{1064\,nm}$ and Ångström exponent (AE'). This procedure is repeated until the difference between the updated AE' and previous AE reduces to a very small value (e.g., 10^{-3}). The final AE is converted to effective radius from the AE-$\bar{r}$ look-up table, and the final values of $\sigma_{532nm},\sigma_{532\,nm},\ \sigma_{1064nm},\sigma_{1064\,nm},$ $S_{532\,nm},S_{1064\,nm}$ and $\bar{r}$ are the retrieved results of this layer. The above iterative algorithm is summarized into Figure 2.

Although in theory, our algorithm can retrieve aerosol extinction and effective radius at each layer, in reality the measurement noise may cause the inversion of certain layers fail to converge. In these cases, we assume that this layer has the same aerosol type and size distribution as its adjacent layer, and then these two layers are combined into a new layer to continue with the inversion.

2.4 Test of the algorithm with synthetic data

For verifying the feasibility of the inversion algorithm, we first conduct some retrieval tests using synthetic data from Mie scattering and radiative transfer simulations. We assume a hypothesized profile of effective radius, backscatter and extinction coefficients of the aerosols, and use the American atmospheric model in 1976 (National Geophysical Data, 1992)(National Geophysical Data, 1992) for molecular scattering, and calculate the attenuated backscatter profiles according to the lidar equation. We then apply our algorithm to retrieve the aerosol property profiles from these simulated lidar signals and compare them with the initial assumptions.

~~To save space, we~~We only present the results for the reflective aerosol model, and results for other aerosol types are similar. The simulated attenuated backscatter profiles for the two wavelengths are shown in Figure 3, and the results of our inversion and their comparison with the assumed profiles are shown in Figure 4. It is clearly seen that the results of the inversion are in good agreement with the assumed profiles. The ~~RRMSE (Relative Root~~ MAPE (Mean ~~Square~~Absolute Percentage Error) between retrieved and assumed profiles of extinction coefficient, average particle effective radius and lidar ratio are all below 0.~~01~~1%, which proves the validity of the algorithm in theory. Note that typically, selection of aerosol type is critical as incorrect assumption of aerosol refractive index will result in divergence of the algorithm and thus yield no valid retrieval. -This also helps us to determine the appropriate aerosol type, i.e., the type that yields the best retrieval results.

3 Application to real lidar measurements

Before applying our algorithm to CALIOP measurements, we first use Raman lidar measurements to test its accuracy as Raman lidars can directly retrieve aerosol extinction profiles without assuming a lidar ratio.

3.1 Application to Raman lidar measurements

A Raman lidar (Model LR231-D300, Raymetrics S.A, Greece) is installed on top of an 8-floor building at the Peking University site (39°59′N, 116°18′E, 53m above sea level). It can provide the extinction and backscatter coefficient at ~~532*nm*~~532 *nm* by Raman inversion (Ansmann et al., 1990) without the need to assume the lidar ratio. To test our inversion algorithm, we apply it to the elastic backscatter signals at 532 and ~~1064nm~~1064 nm and compare the retrieved extinction profile at ~~532nm~~532 nm with that retrieved with the Raman method. ~~but~~But an approximation of AE is used in the inversion at ~~1064*nm*.~~1064 *nm*, that we approximate the 355 ~ 532 nm AE as the 532 ~ 1064 nm AE to calculate extinction profile at 1064 nm by Eq. (10). We applicate the modified inversion algorithm to the cases of four different aerosol types. To facilitate the determination of the initial value, we use the mothed of remodelling downward attenuated

backscatter from ground-based lidar ~~(Tao et al., 2008)~~(Tao et al., 2008) to reconstruct the Raman lidar measurements at wavelength of ~~532nm~~532 nm and ~~1064nm~~1064 nm, which are showing Figure 5-8(a).

We examined four cases in December 2017, as shown in Figures 5-8. The cases on 2 and 21 December 2017 both indicate that the extinction coefficient decreases sharply with altitude, and the maximum values occur near the ground (Figure 6b & 7b). The other two cases on December 1 and 23 respectively show the features of an elevated aerosol layer with maximum extinction found above the surface. In all four cases, our retrieval results (red curves) agree well with those retrieved by the Raman method, with ~~RMSE lower than 0.05.~~MAPE less than 30% in extinction coefficient profiles. The lidar ratio profiles retrieved by our algorithm also agree well with obtained from Raman method in some ranges, except these spikes at the highest or lowest point, may be caused by the uncertainty of boundary. The aerosol particle effective radius slightly increases with altitude and the peak (corresponding to ~0.~~1μm~~1 μm) appear at ~0.~~7km~~7 km and ~1.~~7km~~7 km on 1 and 23 December 2017 (Figure 5d & 8d), respectively. Similar results were found by ~~Zhang et al. (2009)~~Zhang et al. (2009) and ~~Cai et al. (2022)~~Cai et al. (2022) with aircraft measurements over Beijing and the Loess Plateau in China respectively, which are mainly associated with long range aerosol transport. The variability of particle effective radius profiles in Figure 6d is a typical feature for low (and stable) PBL (Planetary Boundary Layer), which results in both particles and water vapor accumulating near PBL top and thus remarkable hygroscopic growth of particle size may occur ~~(Yang et al., 2020)~~(Yang et al., 2020). The case for Dec 21 (Figure 7d) shows relatively large particle size below~1.4km but sharply decreases. This is likely related to the domination of local pollutions and insignificant PBL temperature inversion ~~(Li et al., 2022; Liu et al., 2009; Zhang et al., 2009)~~(Li et al., 2022; Liu et al., 2009; Zhang et al., 2009).

3.2 Application to CALIOP measurements

We further apply our algorithm to real CALIOP measurements. To test its performance, we collocate CALIOP profiles with those from surface-based Raman lidar measurement within the European Aerosol Research LIdar NETwork (EARLINET, www.earlinet.org, ~~(Matthias et al., 2004)~~(Matthias et al., 2004).

Aerosol profiles from the Napoli (southern Italy, 40.838 °N, 14.183 °E, ~~118m~~118 m above sea level), Evora (south-central Portugal, 38.5678 °N, −7.9115 °E, ~~293m~~293 m above sea level) and Warsaw (east-central, 52.21 °N, 20.98 °E, 112m above sea level) stations have the best match with CALIOP and high data quality in cloudless sky, are primarily used to validate the retrieval results. The CALIPSO overpass times for the chosen cases and the corresponding horizontal distances between the sub-satellite point and ground-based Raman lidar site are listed in Table 2.

To compare with the lidar returns measured by CALIOP (down-looking) and ground-based Raman lidar (up-looking), we still use the mothed of remodelling downward attenuated backscatter from ground-based lidar ~~(Tao et al., 2008)~~(Tao et al., 2008) to reconstruct the downward attenuated backscatter signals for the ground-based Raman lidar. The attenuated backscatter signals of CALIOP was averaged for 163 nearby sub-satellite point profiles (CALIPSO ground track range of about ~~30km~~30 km within ~~8s~~8 s) ~~(Lu et al., 2011; Wang et al., 2007)~~(Lu et al., 2011; Wang et al., 2007), obtained from CALIOP level 1B products, to improve the signal-to-noise ratio.

The attenuated backscatter profiles at ~~532*nm*~~532 nm from CALIOP agree well with those from the Napoli Raman Lidar (NRL), as shown in Figures 9-14(a). The initial altitude of inversion (the upper boundary of the aerosol layer) is determined by the variation of attenuated backscatter signal and volume linear depolarization ratio at ~~532*nm*~~532 nm. Comparison between our inversion results, CALIOP operational results and Raman results is shown in Figure 9-14(c).

The CALIOP operational product only provides retrievals for three cases considered, namely 20 August 2006, 20 June 2007 and 22 July 2007. In all three cases, the aerosol extinction profiles of our algorithm (red curve) appear in better consistency with Raman lidar results~~.~~, and our algorithm cut the mean MAPE between the retrieval of extinction profiles in CALIOP and Raman lidar from 74% (CALIOP operational product) to 37%. Our algorithm successfully corrects the overestimation for the August 20, 2006 and July 22, 2007 cases. For the June 20, 2007 case, the operational results show a lower peak at ~1.~~7km~~7 km and a secondary peak at ~~4km~~4 km, both of which are absent in the Raman profile, and our results agree

well with Raman in both the shape and magnitude. In the other three cases, CALIOP does not provide Level 2 retrieval results. Our algorithm is able to retrieve and the extinction profiles agree well with Raman lidar observations. Our retrievals do show more fluctuations compared to Raman lidar, possibly due to the noises in the attenuated backscatter profiles of CALIOP. Because Raman lidar does not provide retrieval of aerosol effective radius profiles, we compare the lidar ratio profiles by our algorithm and the Raman algorithm. Overall, our algorithm produces lidar ratios varying in a relatively small range around 50, whereas Raman lidar ratios can vary from ~10 to 200. Also, the Raman lidar ratios tend to change sharply at the highest or lowest point, which may be caused by the inversion errors at the boundary. By removing these spikes, the differences of the lidar ratio between CALIOP and Raman is obviously reduced. In general, the aerosol particle effective radius increases with altitude, similar to Figures 5d and 8d, but the fluctuations of the profiles may also be caused the noise in the CALIOP measurement.

When examining the CALIOP backscatter measurements, we found that the backscatter signal at ~~1064nm~~1064 nm is often stronger than that at ~~532nm~~532 nm after 2010, which is unphysical and possibly due to issues such as calibration and lidar degradation. As a result, the remodeled backscatter profiles of CALIOP appear noisier and do not exactly match those from Raman lidar for the Evora and Warsaw stations, which only have collocated measurements in 2019 and 2020 (Figure 15-19a). Our retrieved extinction profiles also agree reasonably well with those by Raman lidar (Figure 15-19b), with the lidar ratio profiles and aerosol particle effective radius profiles similar to the cases at Naples. By contrast, the extinction profiles of the official CALIPSO product show large deviations from the Raman profile with unphysical spikes (Figure 16b), incomplete profiles (Figure 17&18b) or no retrievals (Figure 15b).

4 Uncertainty analysis

Uncertainties in aerosol extinction and effective radius profiles ~~from~~retrieved by our two-wavelength inversion algorithm are mainly due to ~~the~~ measurement noise (e.g., the signal statistical error, the estimations of molecular optical properties, etc.), calibration errors, and assumption errors ~~(e.g., single-scatter~~

~~approximation) and the look-up table.~~. In this section, we ~~mainly analyze~~further examine the errors associated with the ~~look-up table~~assumptions in the algorithm.

~~Since the value of AE, which is the key variable in the iterative process, is obtained from the look-up table, the errors on the hypothesis of aerosol refractive index, size distribution and shape in each aerosol layer will affect the variability of lidar ratio in solving the lidar equation. Figure 20 shows the relationship between spherical aerosol particle radius and AE in different aerosol refractive indices. For aerosol particles with the same size, the real part of the refractive index (m_r) mainly affects the cycle period of AE, and the imaginary part (m_i) directly impacts its range of variability. In addition, AE is not quite sensitive to coarse particles, which limit the applicability of our algorithm primarily to fine mode aerosols. The spherical assumption also adds to the uncertainty in the existence of non-spherical particles, such as dust.~~

~~Although the significant difference of these six aerosol types in look-up table can ensure the reasonable inversion result come from a specific aerosol type, the limited look-up table also restrict the inversion of other aerosol types. As the different type of aerosols in the aerosols optical parameters database of CEOS-Chem (http://wiki.seas.harvard.edu/geos-chem) show that the relative change of complex imaginary parts of refractive index is greater than its real parts (e.g. at $532nm$: $1.3 < m_r < 1.7$ & $0 < m_i < 0.4$), which tells our look-up table need to pay more attention to the complex imaginary parts of refractive index in the future.~~

First, the single-scattering approximation is used in solving lidar equation, as multiple scattering effects in aerosol layers are generally small and are currently neglected for CALIOP (Winker et al., 2009). We limit the application of our algorithm to clear sky weather conditions to reduce this error, but this error is very difficult to quantify.

Second, the errors in the aerosol refractive index, size distribution and spherity assumptions in look-up tables can also introduce errors in solving the lidar equation. The lognormal distribution assumption of aerosol volume-size distribution may make the algorithm fail to converge in other actual size distributions. For example, using data generated by Junge distribution (a simpler aerosol size distribution), the algorithm

cannot yield valid retrieval results. Similar outcome is noted for non-spherical particles or aerosol types significantly different from the assumed type.

Finally, we consider assumption and retrieval uncertainties as a perturbation in the lidar ratio and attempt to quantify its effect on the retrieved profiles. We increase the lidar ratio profiles at 532 nm and 1064 nm from the look-up tables by ±10% before calculating the synthetic attenuated backscatter profiles, which makes the synthetic data do not entirely match the look-up table. The retrieval profiles exhibit mean MAPE less than 14% (in 10% case) and 17% (in -10% case), indicating that the algorithm is comparatively robust to noise.

5 Summary and discussion

In this study, we described a modified lidar inversion algorithm to retrieve aerosol extinction and size distribution simultaneously from two wavelengths elastic lidar measurements. Its major advantage over the operational CALIOP algorithm is that the lidar ratio of each layer is determined iteratively by the lidar ratio-AE look-up table. The algorithm was applied to the ground-based Raman lidar measurements at the PKU site, as well as to CALIOP measurements. The comparison results indicate that the retrieved aerosol extinction coefficient profiles by our method using CALIOP attenuated backscatter measurements are in good agreement with Raman lidar measurements. Characteristics of aerosol effective radius profiles are also retrieved, which can be used as a reference for aerosols size information.

In comparison with the iterative method by transcendental equation (Ackermann, 1997, 1998), our inversion uses the look-up table to simplify the complex calculation. Cao et al. (2019) develop a lidar-ratio iteration method to invert the particle-size distribution with assumed Junge distribution, but the method was just used in simple simulation without actual tests. ~~Although Lu et al. (2011)~~Although Lu et al. (2011) invert the aerosol backscatter coefficient profiles from CALIPSO lidar measurements by iterative method, failed to consider the size distribution of aerosols which may introduce uncertainties in the inversion. Compared with

other modified CALIOP inversions by combining other measurements, such as ground-based lidar ~~(Wang et al., 2007)~~(Wang et al., 2007), our inversion is weaker by the space-time limitations.

However, this study still bears certain limitations. The current algorithm is primarily suitable for fine mode spherical particles, such as urban pollution, and considers the change of aerosol size (thus lidar ratio) with altitude, due to long range transport, vertical mixing, hygroscopic growth, etc. Non-spherical particles such as dust will be explored in the next step, ~~possible~~possibly by taking advantage of the depolarization ratio (Gialitaki et al., 2020; Kahnert et al., 2020; Luo et al., 2022; Luo et al., 2019) measurement that is not used here. Another drawback is that although the algorithm does not need to assume a lidar ratio, the complex refractive index still needs to be assumed. As discussed above, the lidar ratio is very sensitive to the imaginary part and an incorrect assumption may induce errors or even makes the algorithm unable to converge. Therefore, this algorithm is mostly suitable when there is no significant change in aerosol type vertically. Finally, the polarization channel of CALIOP may contain additional aerosol type information but is only used when determining the initial refractive index (excluding dust) here. We also plan to refine our look-up table by incorporating polarization in order to improve the accuracy of the retrieval.

Data availability

All raw data can be provided by the corresponding authors upon request.

Author contributions

LC and JL planned the research; LC, JL, JR, CX, and LZ developed the algorithm; LC and JL analyzed the results; LC and JL wrote the manuscript.

Competing interests

The authors declare that they have no conflict of interest.

Acknowledgement

This study is funded by National Natural Science Foundation of China (NSFC) Grant No. 42175144.

References

Ackermann, J.: Two-wavelength lidar inversion algorithm for a two-component atmosphere, Appl. Opt., 36, 5134-5143, 10.1364/AO.36.005134, 1997.

Ackermann, J.: Two-wavelength lidar inversion algorithm for a two-component atmosphere with variable extinction-to-backscatter ratios, Appl. Opt., 37, 3164-3171, 10.1364/AO.37.003164, 1998.

Ansmann, A., Riebesell, M., and Weitkamp, C.: Measurement of atmospheric aerosol extinction profiles with a Raman lidar, Opt. Lett., 15, 746-748, 10.1364/OL.15.000746, 1990.

Bodhaine, B. A., Wood, N. B., Dutton, E. G., and Slusser, J. R.: On Rayleigh Optical Depth Calculations, Journal of Atmospheric and Oceanic Technology, 16, 1854-1861, 10.1175/1520-0426(1999)016<1854:orodc>2.0.co;2, 1999.

Burton, S. P., Ferrare, R. A., Hostetler, C. A., Hair, J. W., Rogers, R. R., Obland, M. D., Butler, C. F., Cook, A. L., Harper, D. B., and Froyd, K. D.: Aerosol classification using airborne High Spectral Resolution Lidar measurements – methodology and examples, Atmos. Meas. Tech., 5, 73-98, 10.5194/amt-5-73-2012, 2012.

Cai, Z., Li, Z., Li, P., Li, J., Sun, H., Yang, Y., Gao, X., Ren, G., Ren, R., and Wei, J.: Vertical distributions of aerosol microphysical and optical properties based on aircraft measurements made over the Loess Plateau in China, Atmospheric Environment, 270, 118888, https://doi.org/10.1016/j.atmosenv.2021.118888, 2022.

Cao, N., Yang, S., Cao, S., Yang, S., and Shen, J.: Accuracy calculation for lidar ratio and aerosol size distribution by dual-wavelength lidar, Applied Physics A, 125, 590, 10.1007/s00339-019-2819-y, 2019.

Deshler, T., Hervig, M. E., Hofmann, D. J., Rosen, J. M., and Liley, J. B.: Thirty years of in situ stratospheric aerosol size distribution measurements from Laramie, Wyoming (41°N), using balloon-borne instruments, Journal of Geophysical Research: Atmospheres, 108, 10.1029/2002jd002514, 2003.

Eswaran, K., Satheesh, S. K., and Srinivasan, J.: Sensitivity of aerosol radiative forcing to various aerosol parameters over the Bay of Bengal, Journal of Earth System Science, 128, 170, 10.1007/s12040-019-1200-z, 2019.

Fernald, F. G.: Analysis of atmospheric lidar observations: some comments, Appl. Opt., 23, 652-653, 10.1364/AO.23.000652, 1984.

Gialitaki, A., Tsekeri, A., Amiridis, V., Ceolato, R., Paulien, L., Kampouri, A., Gkikas, A., Solomos, S., Marinou, E., Haarig, M., Baars, H., Ansmann, A., Lapyonok, T., Lopatin, A., Dubovik, O., Groß, S., Wirth, M., Tsichla, M., Tsikoudi, I., and Balis, D.: Is the near-spherical shape the "new black" for smoke?, Atmos. Chem. Phys., 20, 14005-14021, 10.5194/acp-20-14005-2020, 2020.

Goto, D., Nakajima, T., Takemura, T., and Sudo, K.: A study of uncertainties in the sulfate distribution and its radiative forcing associated with sulfur chemistry in a global aerosol model, Atmos. Chem. Phys., 11, 10889-10910, 10.5194/acp-11-10889-2011, 2011.

Hara, K., Nishita-Hara, C., Osada, K., Yabuki, M., and Yamanouchi, T.: Characterization of aerosol number size distributions and their effect on cloud properties at Syowa Station, Antarctica, Atmos. Chem. Phys., 21, 12155-12172, 10.5194/acp-21-12155-2021, 2021.

He, Q., Li, C., Geng, F., Zhou, G., Gao, W., Yu, W., Li, Z., and Du, M.: A parameterization scheme of aerosol vertical distribution for surface-level visibility retrieval from satellite remote sensing, Remote Sensing of Environment, 181, 1-13, https://doi.org/10.1016/j.rse.2016.03.016, 2016.

Hostetler, C., Liu, Z., Reagan, J., Vaughan, M., Winker, D., Osborn, M., Hunt, W., Powell, K., and Trepte, C.: CALIOP algorithm theoretical basis document calibration and Level 1 data products, Hampton, VA: NASA Langley Research Center, 2006.

IPCC: Climate Change 2021 – The Physical Science Basis: Working Group I Contribution to the Sixth Assessment Report of the Intergovernmental Panel on Climate Change, Cambridge University Press, Cambridge, DOI: 10.1017/9781009157896, 2023.

Josset, D., Rogers, R., Pelon, J., Hu, Y., Liu, Z., Omar, A., and Zhai, P.-W.: CALIPSO lidar ratio retrieval over the ocean, Opt. Express, 19, 18696-18706, 10.1364/OE.19.018696, 2011.

Kahnert, M., Kanngießer, F., Järvinen, E., and Schnaiter, M.: Aerosol-optics model for the backscatter depolarisation ratio of mineral dust particles, Journal of Quantitative Spectroscopy and Radiative Transfer, 254, 107177, https://doi.org/10.1016/j.jqsrt.2020.107177, 2020.

Klett, J. D.: Lidar inversion with variable backscatter/extinction ratios, Appl. Opt., 24, 1638-1643, 10.1364/AO.24.001638, 1985.

Kudo, R., Nishizawa, T., and Aoyagi, T.: Vertical profiles of aerosol optical properties and the solar heating rate estimated by combining sky radiometer and lidar measurements, Atmos. Meas. Tech., 9, 3223-3243, 10.5194/amt-9-3223-2016, 2016.

Li, Y., Guo, X., Jin, L., Li, P., Sun, H., Zhao, D., and Ma, X.: Aircraft Measurements of Summer Vertical Distributions of Aerosols and Transitions to Cloud Condensation Nuclei and Cloud Droplets in Central Northern China, Chinese Journal of Atmospheric Sciences, 46, 845, 10.3878/j.issn.1006-9895.2104.20255, 2022.

Liu, P., Zhao, C., Zhang, Q., Deng, Z., Huang, M., Ma, X., and Tie, X.: Aircraft study of aerosol vertical distributions over Beijing and their optical properties, Tellus B, 61, 756-767, https://doi.org/10.1111/j.1600-0889.2009.00440.x, 2009.

Lu, X., Jiang, Y., Zhang, X., Wang, X., and Spinelli, N.: Two-wavelength lidar inversion algorithm for determination of aerosol extinction-to-backscatter ratio and its application to CALIPSO lidar measurements, Journal of Quantitative Spectroscopy and Radiative Transfer, 112, 320-328, https://doi.org/10.1016/j.jqsrt.2010.07.013, 2011.

Luo, J., Zhang, Q., Luo, J., Liu, J., Huo, Y., and Zhang, Y.: Optical Modeling of Black Carbon With Different Coating Materials: The Effect of Coating Configurations, Journal of Geophysical Research: Atmospheres, 124, 13230-13253, https://doi.org/10.1029/2019JD031701, 2019.

Luo, J., Li, Z., Fan, C., Xu, H., Zhang, Y., Hou, W., Qie, L., Gu, H., Zhu, M., Li, Y., and Li, K.: The polarimetric characteristics of dust with irregular shapes: evaluation of the spheroid model for single particles, Atmos. Meas. Tech., 15, 2767-2789, 10.5194/amt-15-2767-2022, 2022.

Matthias, V., Freudenthaler, V., Amodeo, A., Balin, I., Balis, D., Bosenberg, J., Chaikovsky, A., Chourdakis, G., Comeron, A., Delaval, A., De Tomasi, F., Eixmann, R., Hagard, A., Komguem, L., Kreipl, S., Matthey, R., Rizi, V., Rodrigues, J., Wandinger, U., and Wang, X.: Aerosol lidar intercomparison in the framework of the EARLINET project. 1. Instruments (vol 43, pg 976, 2004), Appl. Opt., 43, 2004.

Mishchenko, M. I. and Yang, P.: Far-field Lorenz–Mie scattering in an absorbing host medium: Theoretical formalism and FORTRAN program, Journal of Quantitative Spectroscopy and Radiative Transfer, 205, 241-252, https://doi.org/10.1016/j.jqsrt.2017.10.014, 2018.

National Geophysical Data, C.: U.S. standard atmosphere (1976), Planetary and Space Science, 40, 553-554, https://doi.org/10.1016/0032-0633(92)90203-Z, 1992.

Potter, J. F.: Two-frequency lidar inversion technique, Appl. Opt., 26, 1250-1256, 10.1364/AO.26.001250, 1987.

Rajeev, K. and Parameswaran, K.: Iterative method for the inversion of multiwavelength lidar signals to determine aerosol size distribution, Appl. Opt., 37, 4690-4700, 10.1364/AO.37.004690, 1998.

Tao, Z., McCormick, M. P., and Wu, D.: A comparison method for spaceborne and ground-based lidar and its application to the CALIPSO lidar, Applied Physics B, 91, 639, 10.1007/s00340-008-3043-1, 2008.

Wang, X., Frontoso, M. G., Pisani, G., and Spinelli, N.: Retrieval of atmospheric particles optical properties by combining ground-based and spaceborne lidar elastic scattering profiles, Opt. Express, 15, 6734-6743, 10.1364/OE.15.006734, 2007.

Winker, D. M., Vaughan, M. A., Omar, A., Hu, Y., Powell, K. A., Liu, Z., Hunt, W. H., and Young, S. A.: Overview of the CALIPSO Mission and CALIOP Data Processing Algorithms, Journal of Atmospheric and Oceanic Technology, 26, 2310-2323, 10.1175/2009jtecha1281.1, 2009.

Yang, J., Li, J., Li, P., Sun, G., Cai, Z., Yang, X., Cui, C., Dong, X., Xi, B., Wan, R., Wang, B., and Zhou, Z.: Spatial Distribution and Impacts of Aerosols on Clouds Under Meiyu Frontal Weather Background Over Central China Based on Aircraft Observations, Journal of Geophysical Research: Atmospheres, 125, e2019JD031915, https://doi.org/10.1029/2019JD031915, 2020.

Zhang, L., Li, J., Jiang, Z., Dong, Y., Ying, T., and Zhang, Z.: Clear-Sky Direct Aerosol Radiative Forcing Uncertainty Associated with Aerosol Optical Properties Based on CMIP6 Models, Journal of Climate, 35, 3007-3019, https://doi.org/10.1175/JCLI-D-21-0479.1, 2022.

Zhang, Q., Ma, X., Tie, X., Huang, M., and Zhao, C.: Vertical distributions of aerosols under different weather conditions: Analysis of in-situ aircraft measurements in Beijing, China, Atmospheric Environment, 43, 5526-5535, https://doi.org/10.1016/j.atmosenv.2009.05.037, 2009.

Table 1. The aerosols parameters of the look-up table. m_r denotes the real part of the refractive index, m_i denotes the imaginary part of the refractive index, and s_d is the standard deviation of the lognormal size distribution.

	Type 1	Type 2	Type 3	Type 4	Type 5	Type 6
m_r (~~532nm~~532 nm)	1.414	1.517	1.380	1.404	1.400	1.452
m_i (~~532nm~~532 nm)	0.0036	0.0234	0.0001	0.0063	0.0050	0.0109
m_r (~~1064nm~~1064 nm)	1.495	1.541	1.380	1.439	1.400	1.512
m_i (~~1064nm~~1064 nm)	0.0043	0.0298	0.0001	0.0073	0.0050	0.0137
s_d	1.4813	1.5624	1.6100	1.5257	1.6000	1.5112

Table 2. Information of collocated EARLINET and CALIPSO cases.

Station	Time (UTC)	Horizontal distance (km)
Napoli	**2006-08-20 01:17:25**	0.0708
	2007-06-20 01:17:57	0.0808
	2008-07-08 01:18:43	0.0690
	2008-08-02 01:13:02	1.3246
	2008-08-09 01:19:14	0.0807
	2009-09-29 01:21:03	0.0778
Evora	**2019-04-05 02:47:48**	0.0863
	2020-01-13 02:54:00	0.0164
	2020-03-18 02:55:43	0.0009
Warsaw	**2015-08-15 01:19:14**	< 0.0001
	2020-03-31 01:13:38	0.0177

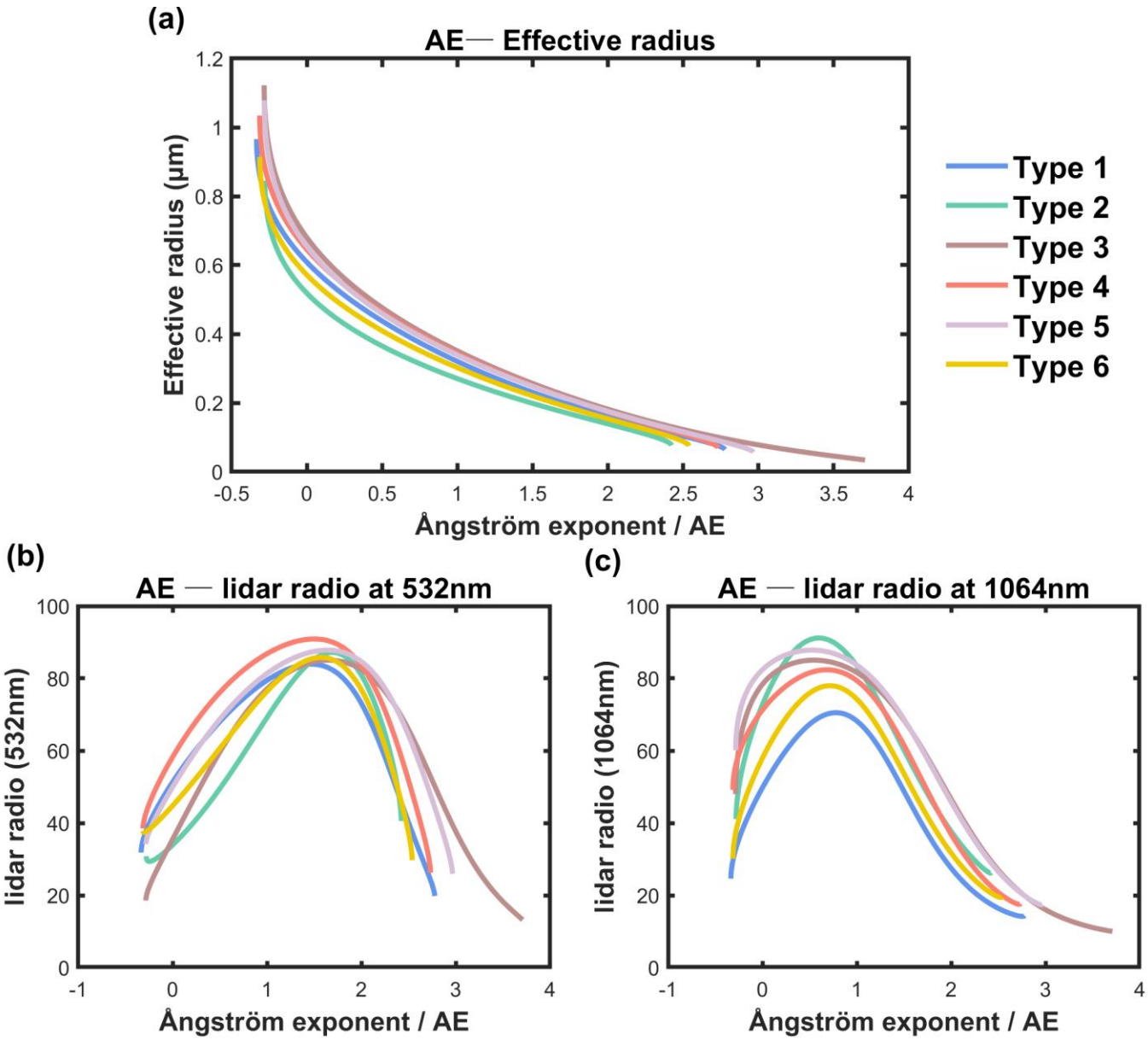

Figure 1. The Look-up tables for (a) AE-effective radius, (b) AE-lidar ratio at ~~532nm~~532 nm532 nm and (c) AE-lidar ratio at ~~1064nm~~1064 nm. The AE is calculated using ~~532nm~~532 nm532 nm and ~~1064nm~~1064 nm aerosol extinction coefficients.

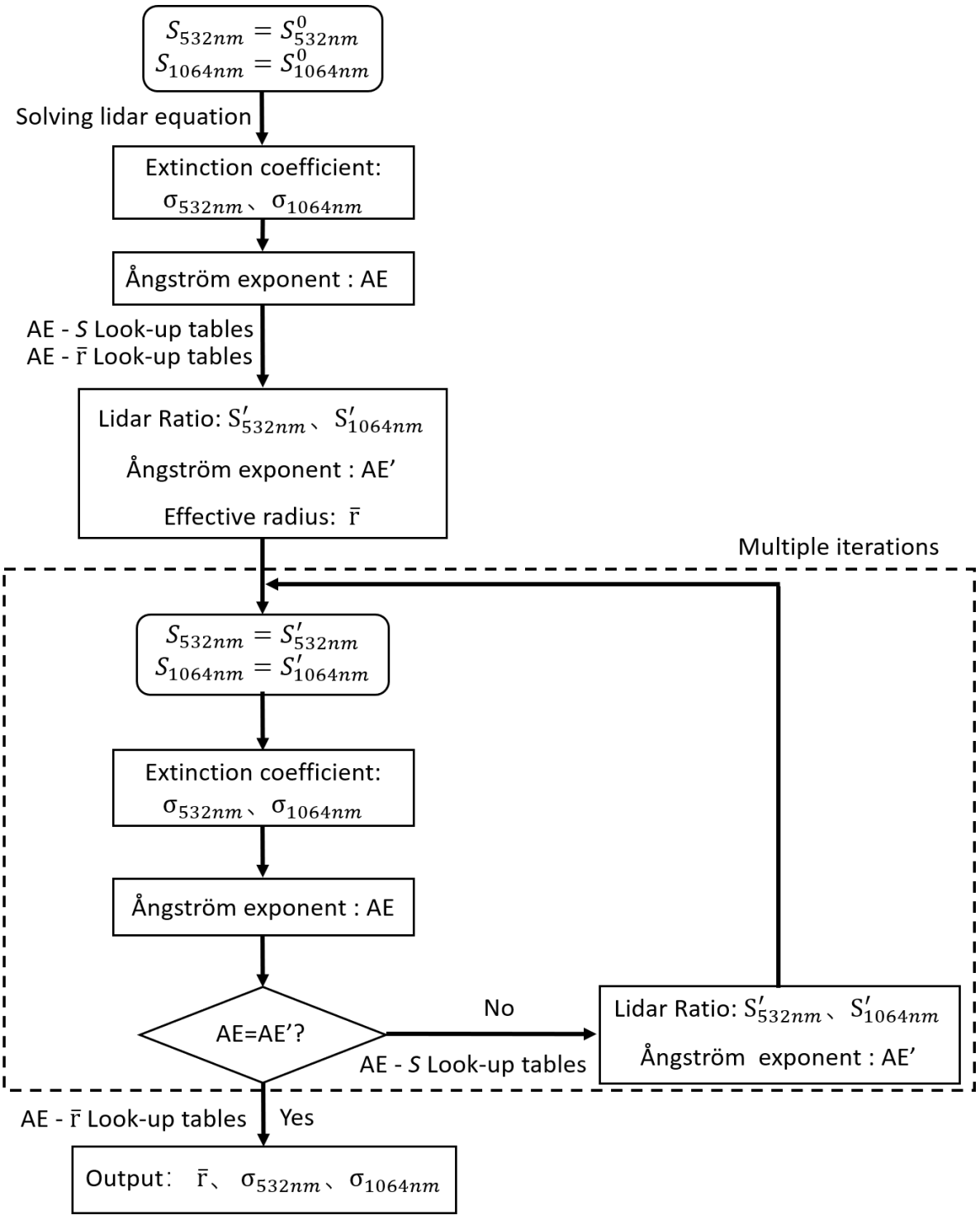

472

473 **Figure 2.** Schematic of the inversion algorithm (λ_1 and λ_2 represent the two different wavelengths,
474 respectively; S is the lidar ratio; σ is the aerosol extinction; AE is the Ångström index; $\bar{r}$ is the average
475 particle effective radius; S^0 is the initial value of lidar ratio; S' and AE′are the look up values of lidar ratio
476 and Ångström index, respectively.)

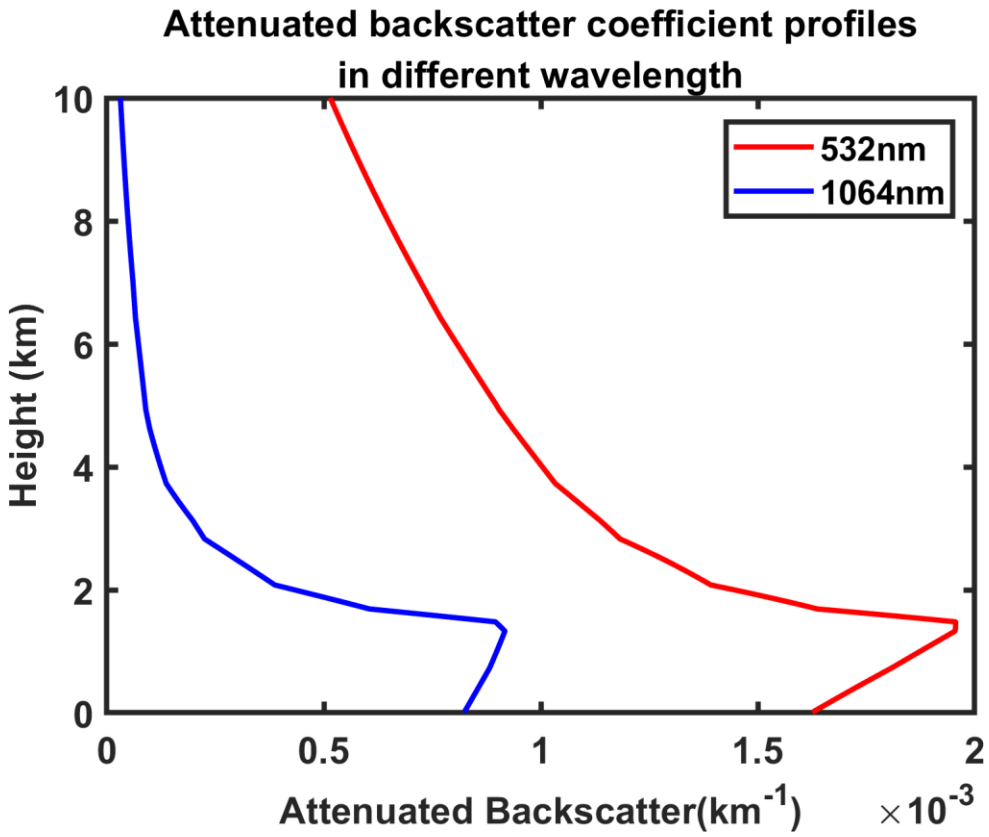

Figure 3. The attenuated backscatter coefficient profiles at different wavelengths using syntheticdata.

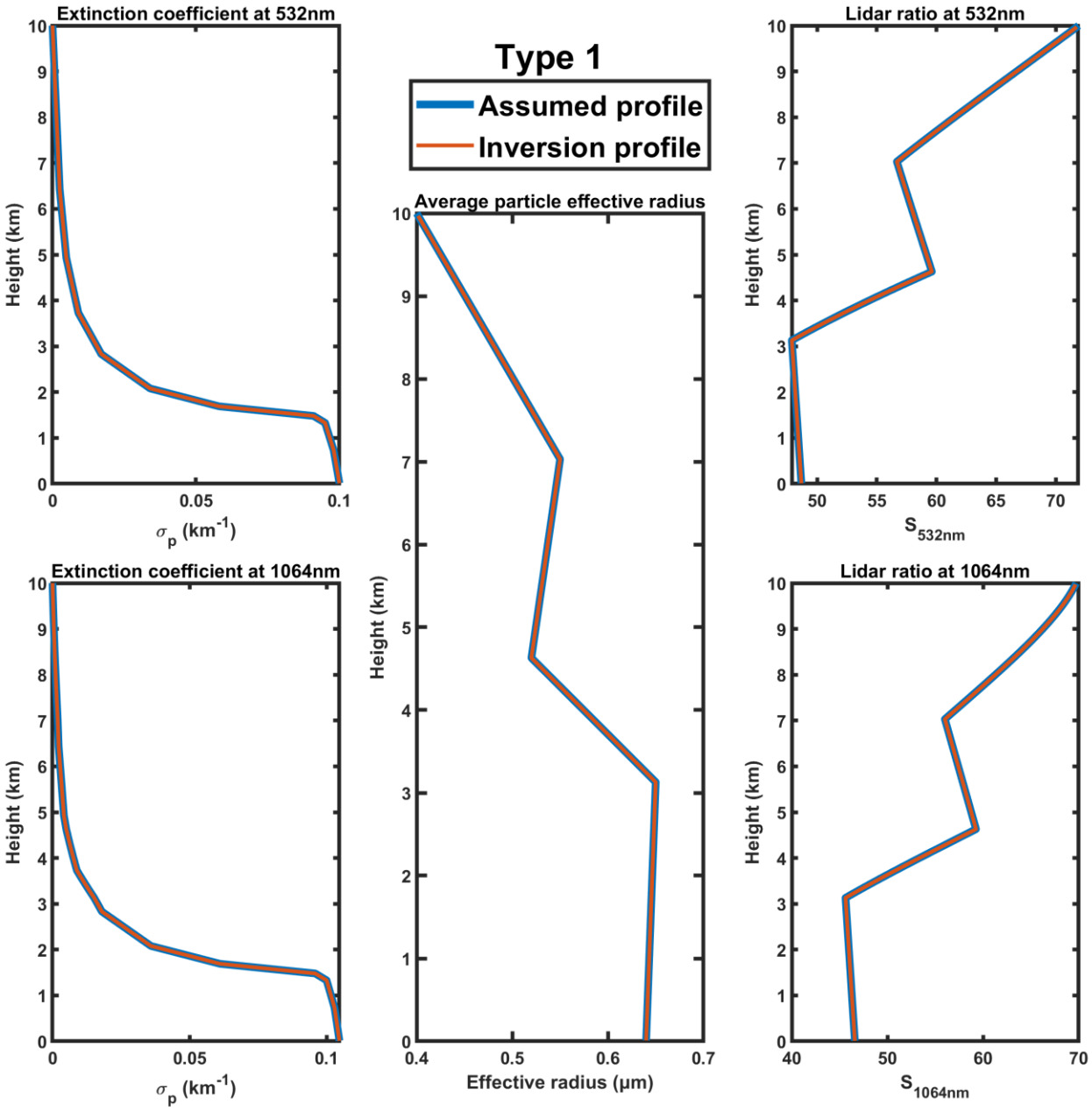

Figure 4. The result of the inversion algorithm using the synthetic data shown in Figure 3.

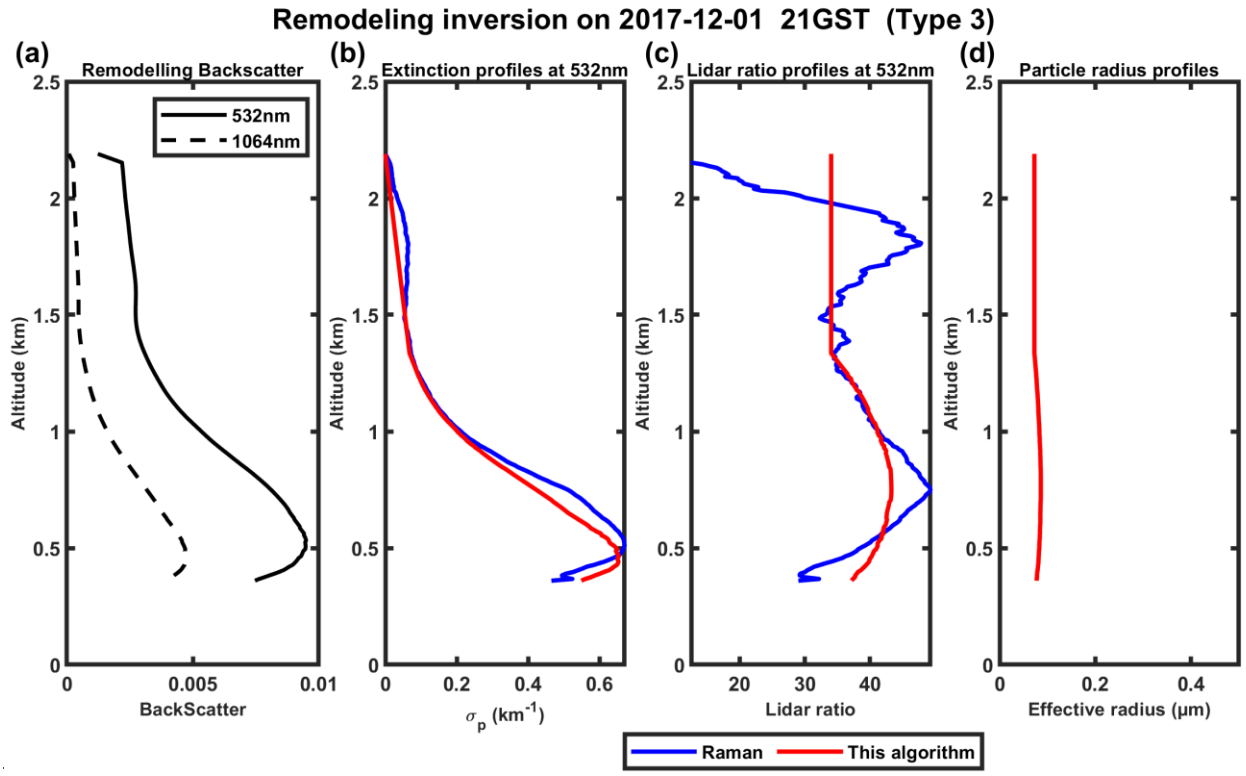
Remodeling inversion on 2017-12-01 21GST (Type 3)
(a)
Remodelling Backscatter
532nm
1064nm
Altitude (km)
BackScatter
(b)
Extinction profiles at 532nm
σ_p (km^{-1})
(c)
Lidar ratio profiles at 532nm
Lidar ratio
(d)
Particle radius profiles
Effective radius (μm)
Raman
This algorithm

481

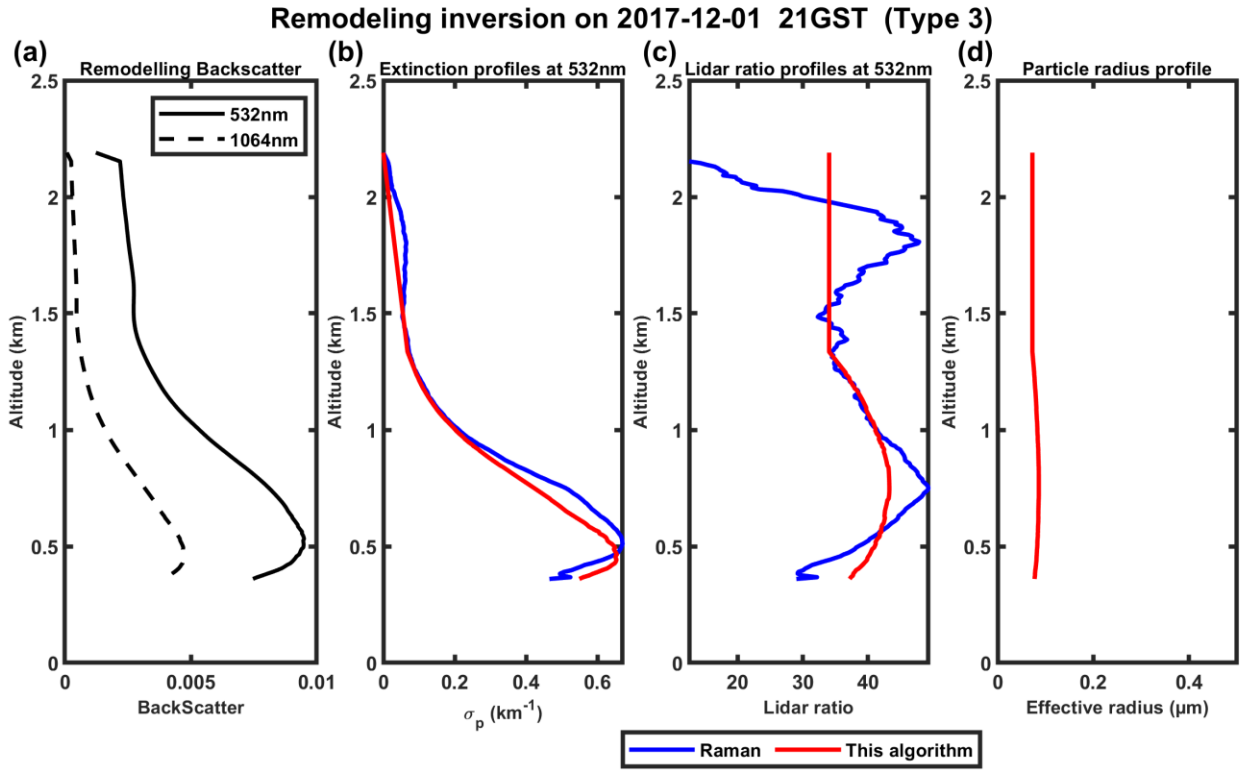
Remodeling inversion on 2017-12-01 21GST (Type 3)
(a)
Remodelling Backscatter
532nm
1064nm
Altitude (km)
BackScatter
(b)
Extinction profiles at 532nm
σ_p (km^{-1})
(c)
Lidar ratio profiles at 532nm
Lidar ratio
(d)
Particle radius profile
Effective radius (μm)
Raman
This algorithm

482

Figure 5. (a) Remodeled downward attenuated backscatter profiles measured by Raman lidar in PKU on 1 December 2017; (b) show the extinction profiles inversed by the modified inversion algorithm (red) and Raman (blue); (c) shows the particle effective radius profiles.

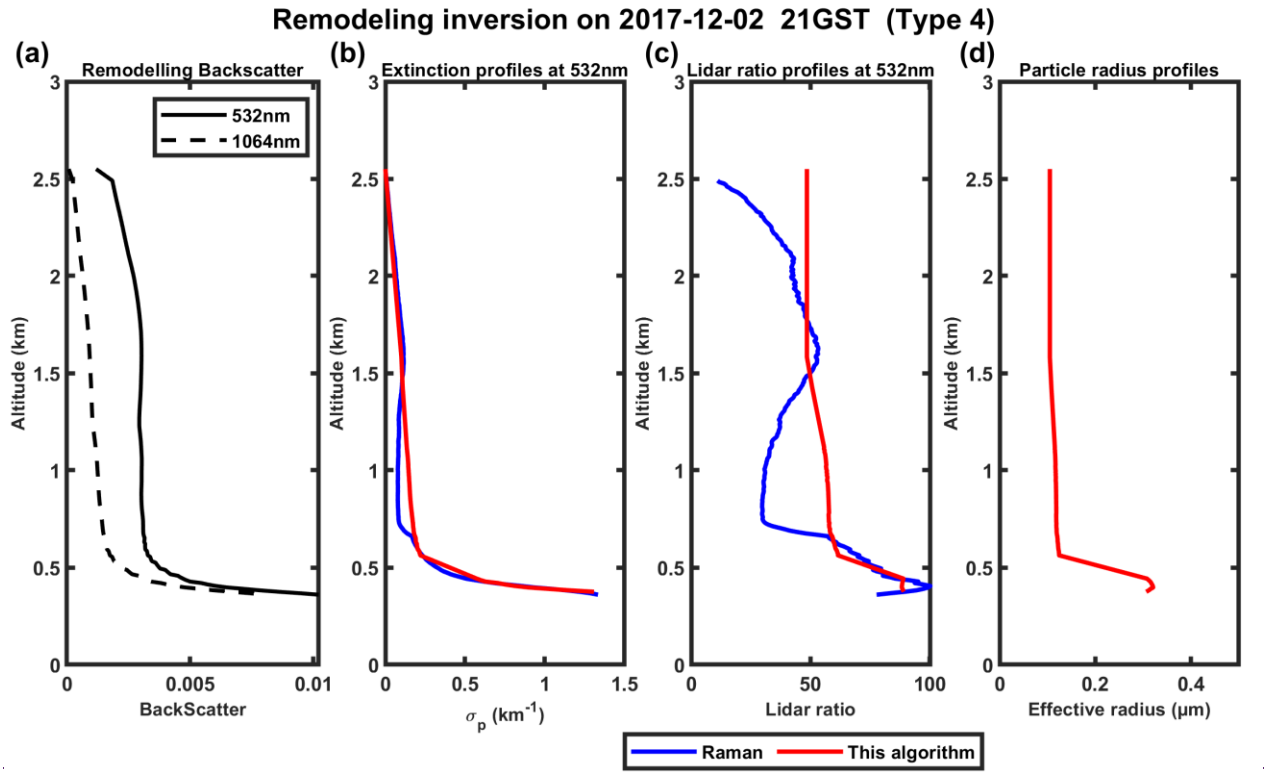

487

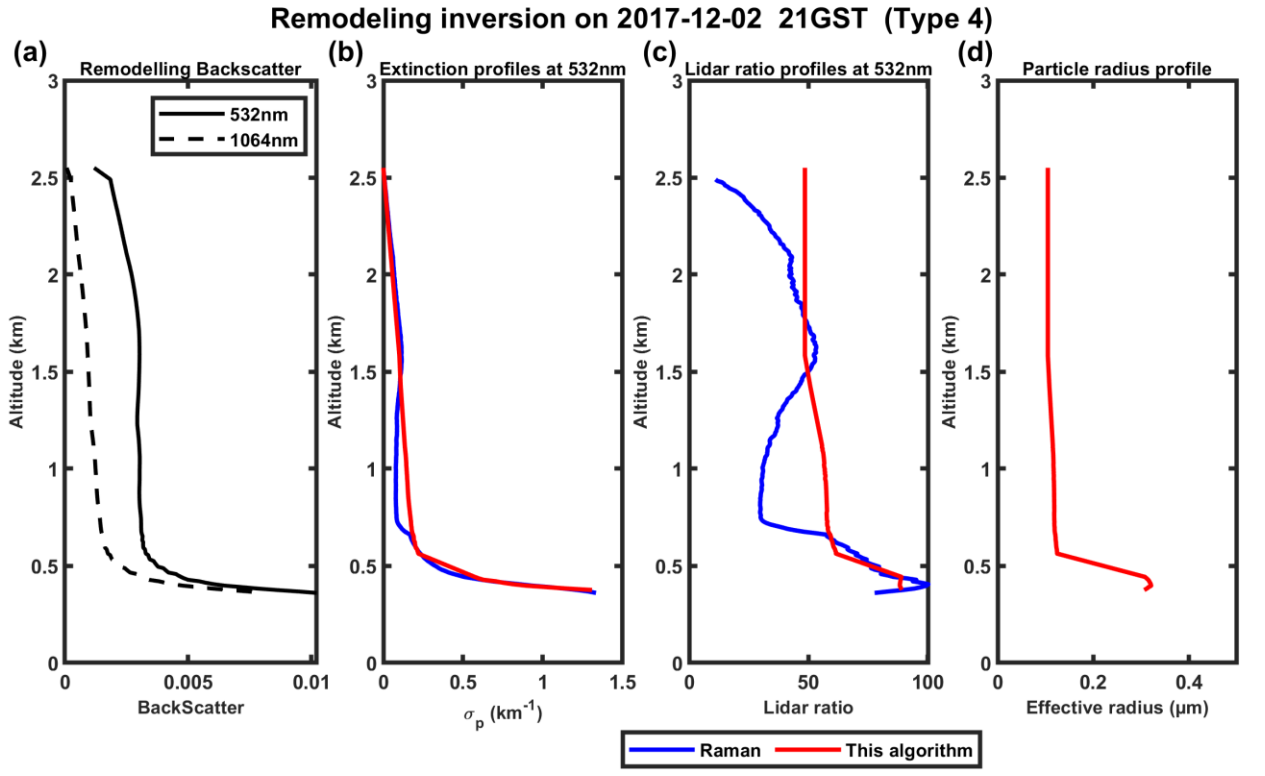

488

489 **Figure 6.** Same as Figure 5 but on 2 December 2017.

490

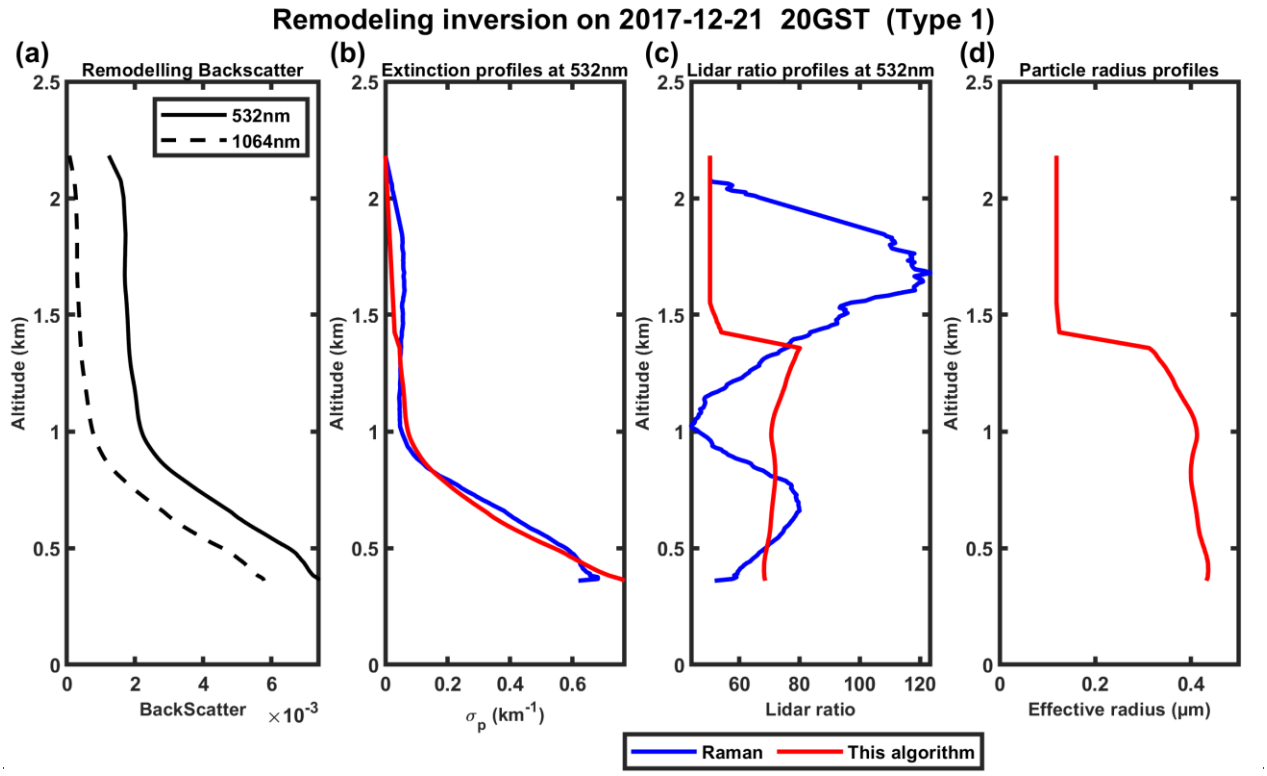

491

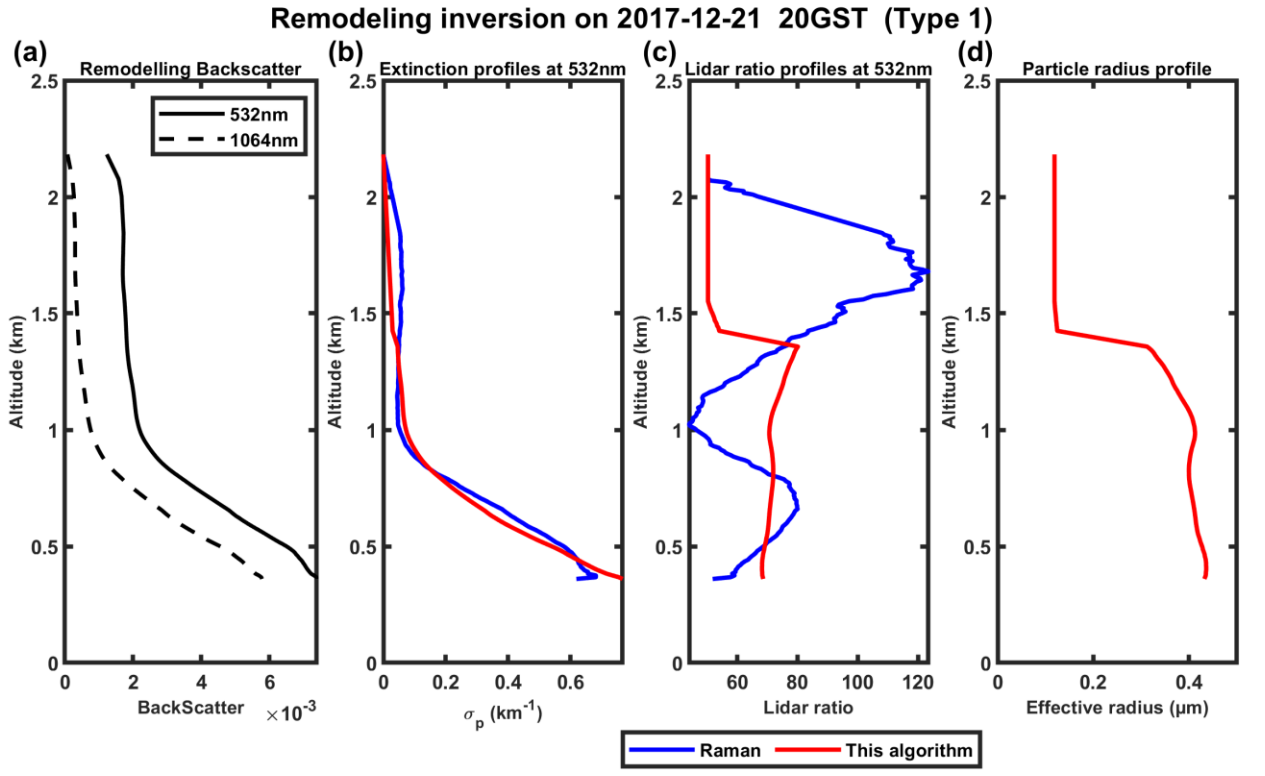

492

493 **Figure 7.** Same as Figure 5 but on 21 December 2017.

494

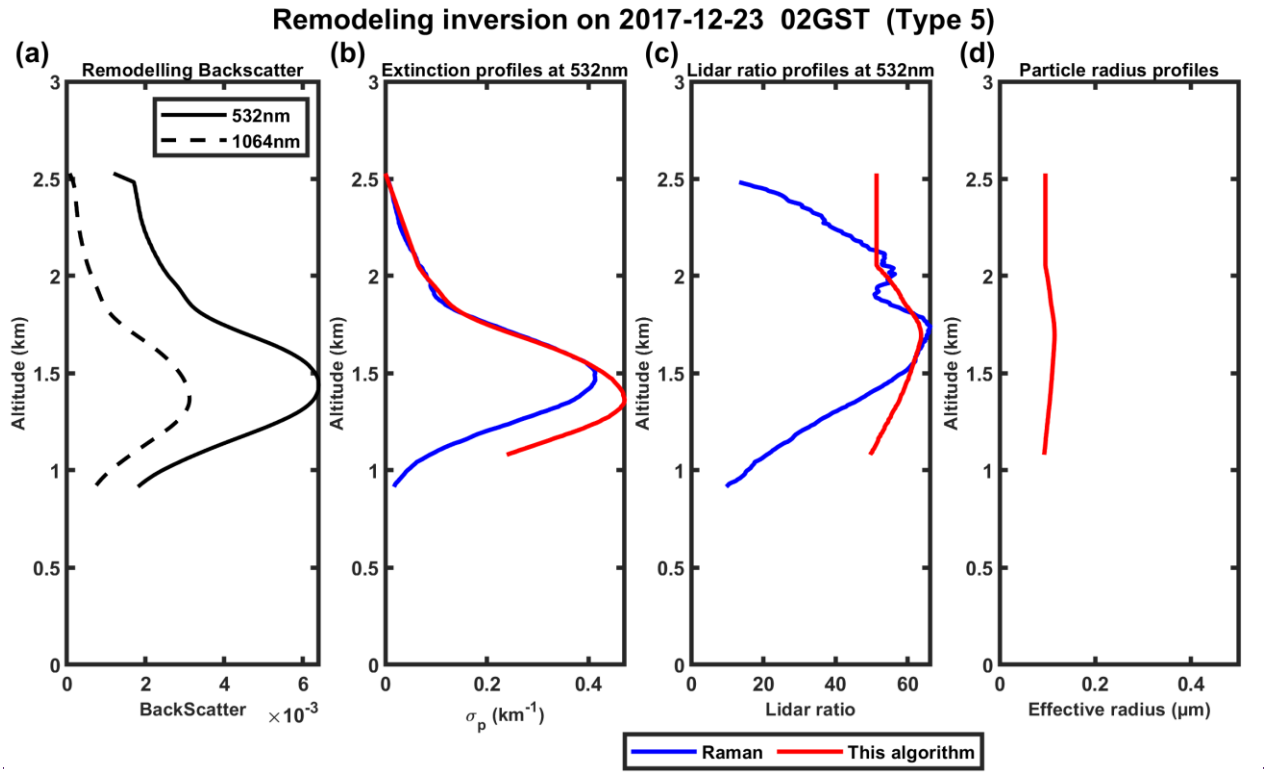

495

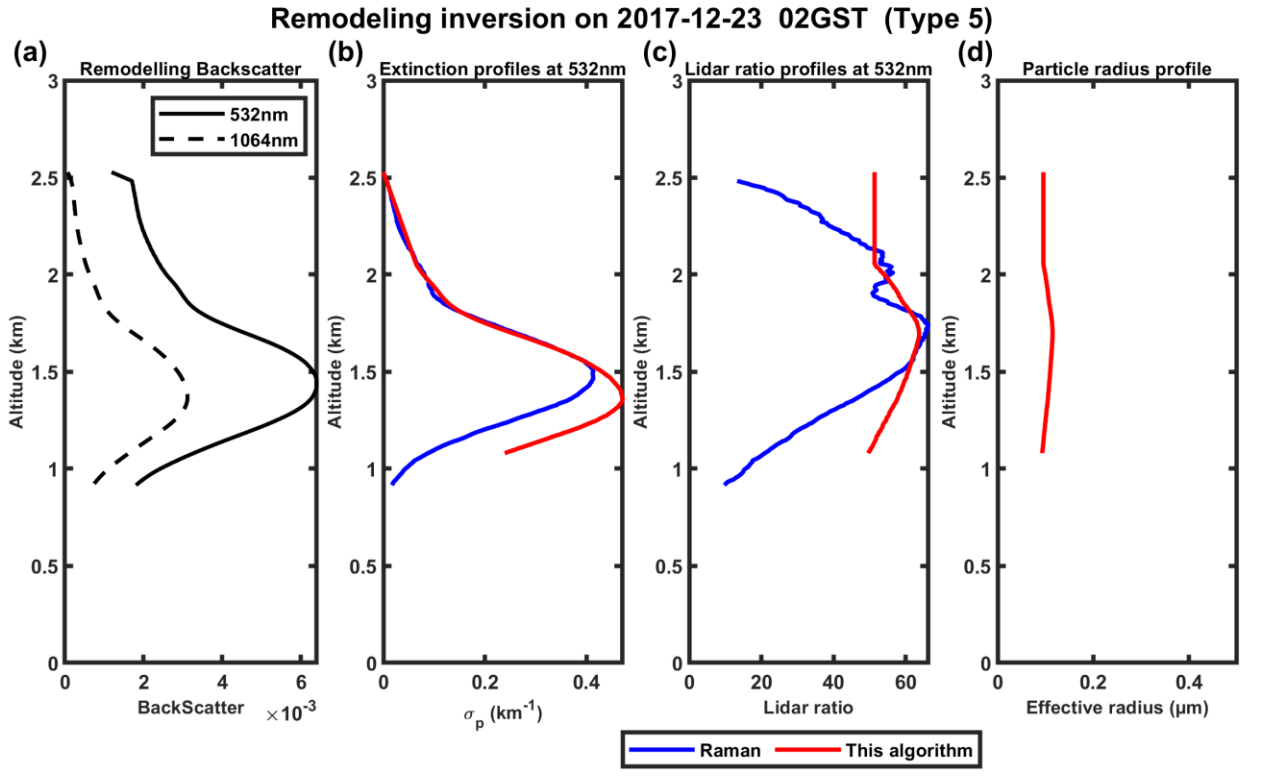

496

497 **Figure 8.** Same as Figure 5 but on 23 December 2017.

498

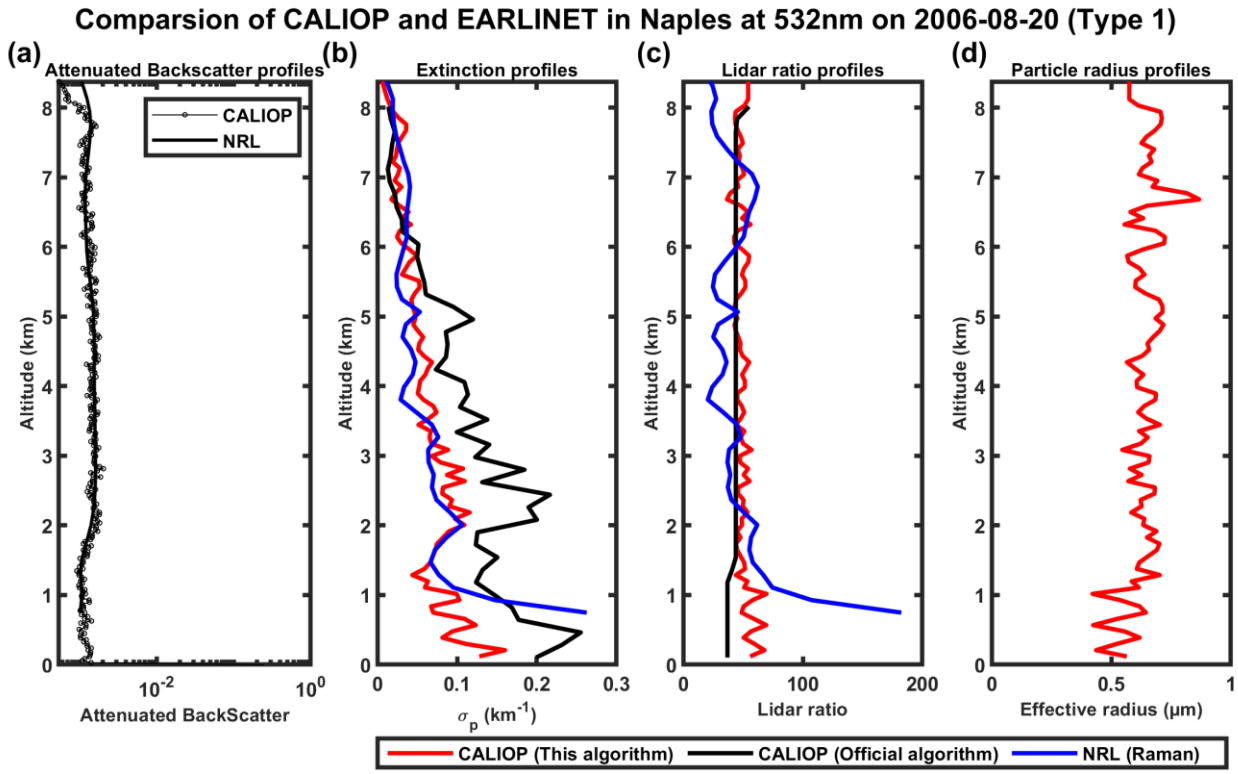

499

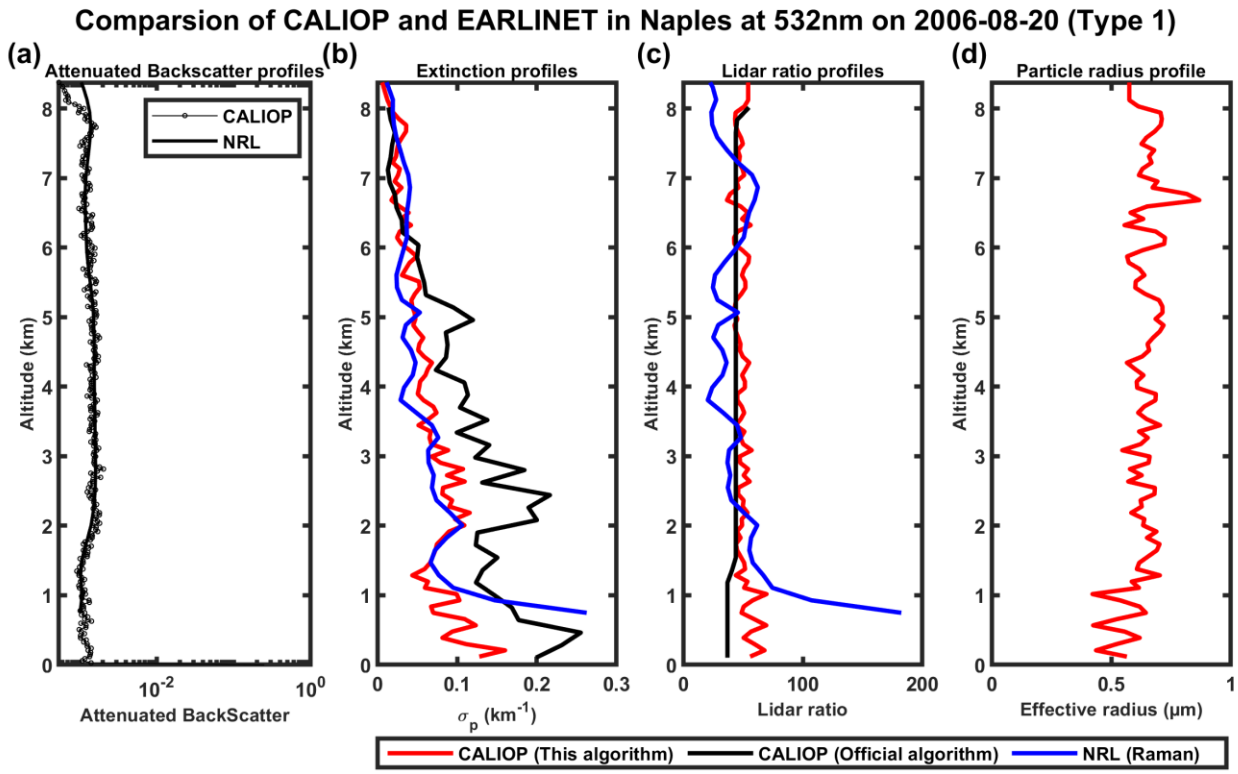

500

501 **Figure 9.** ~~532nm~~532 nm and ~~106~~1064 nm attenuated backscatter profiles measured by CALIOP (black solid

502 line with circle marker) and NRL (remodeling, black solid line) on 20 August 2006 in logarithmic scale in

503 horizontal direction (a); (b, c, d) show the extinction profiles, lidar ratio profiles and particle radius profiles,
504 respectively, provided by our inversion algorithm (red), CALIOP operational level 2 product (black) and
505 EARLINET level 2 product (blue).

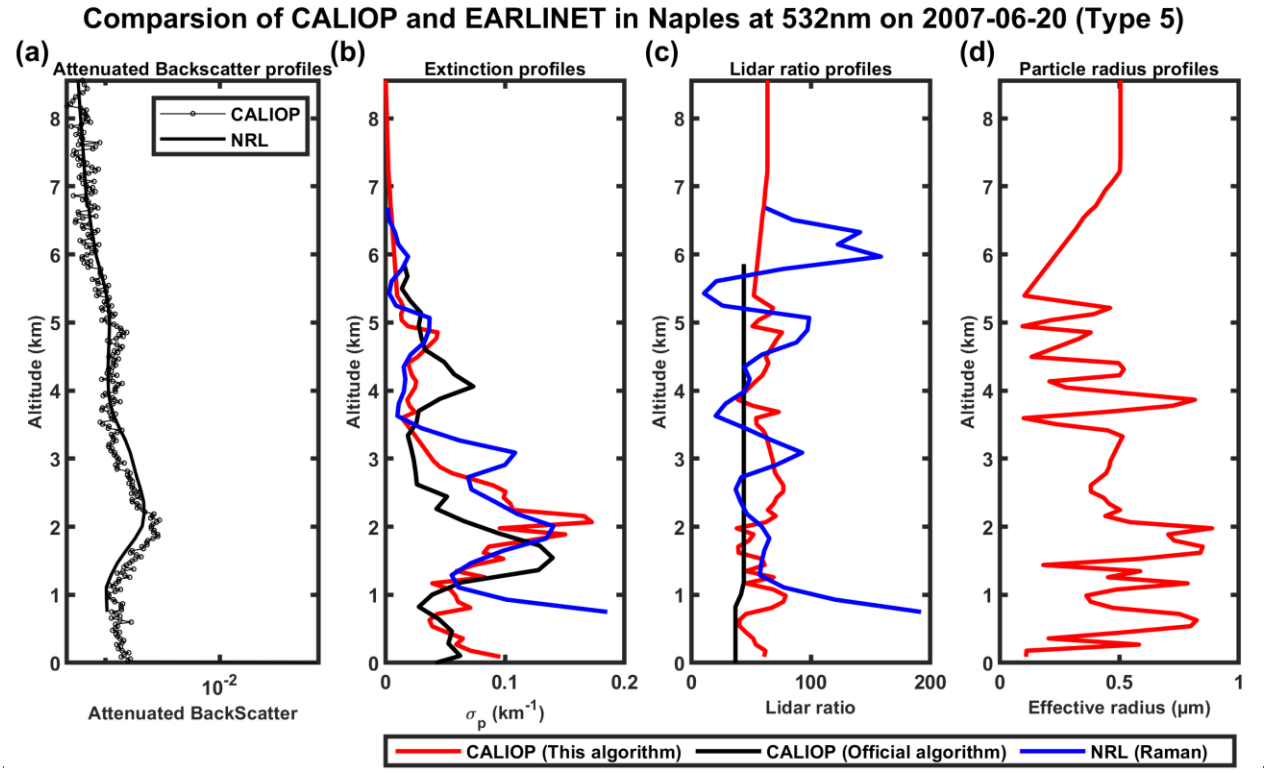

506

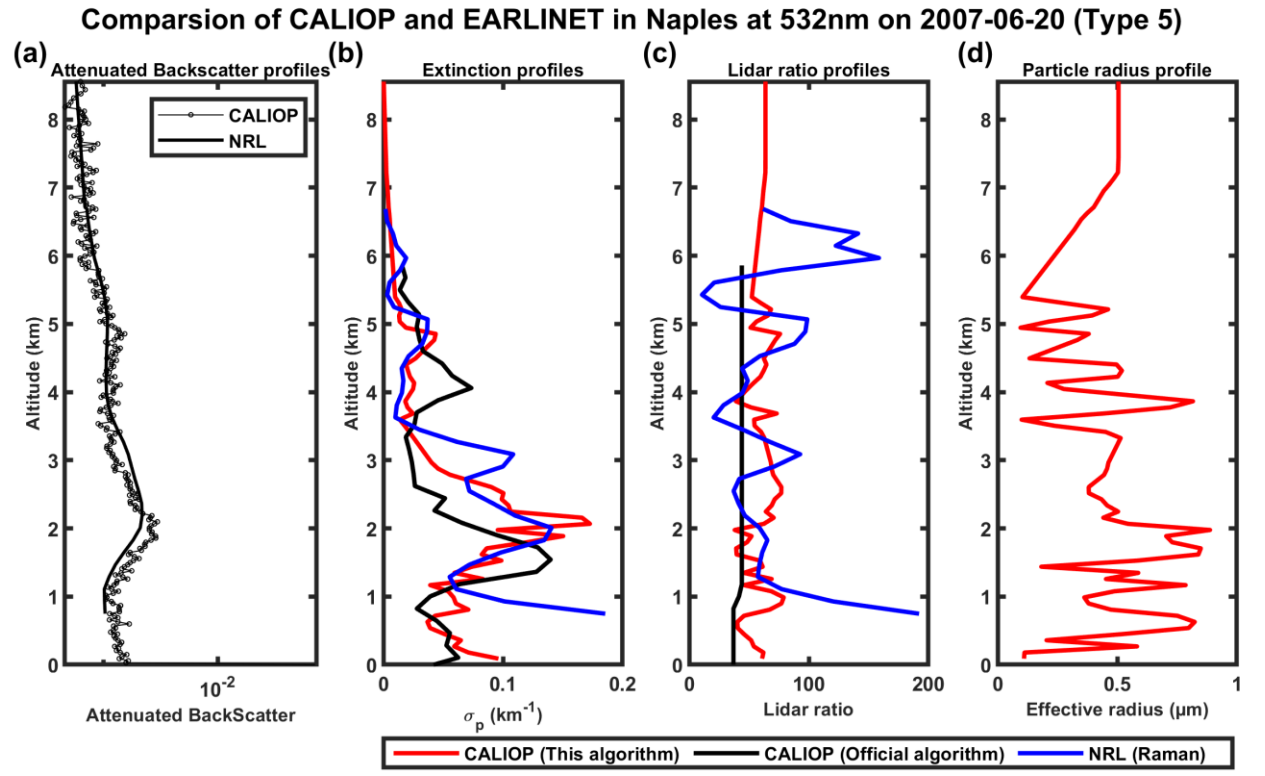

507

508 **Figure 10.** Same as Figure 9 but on 20 June 2007.

509

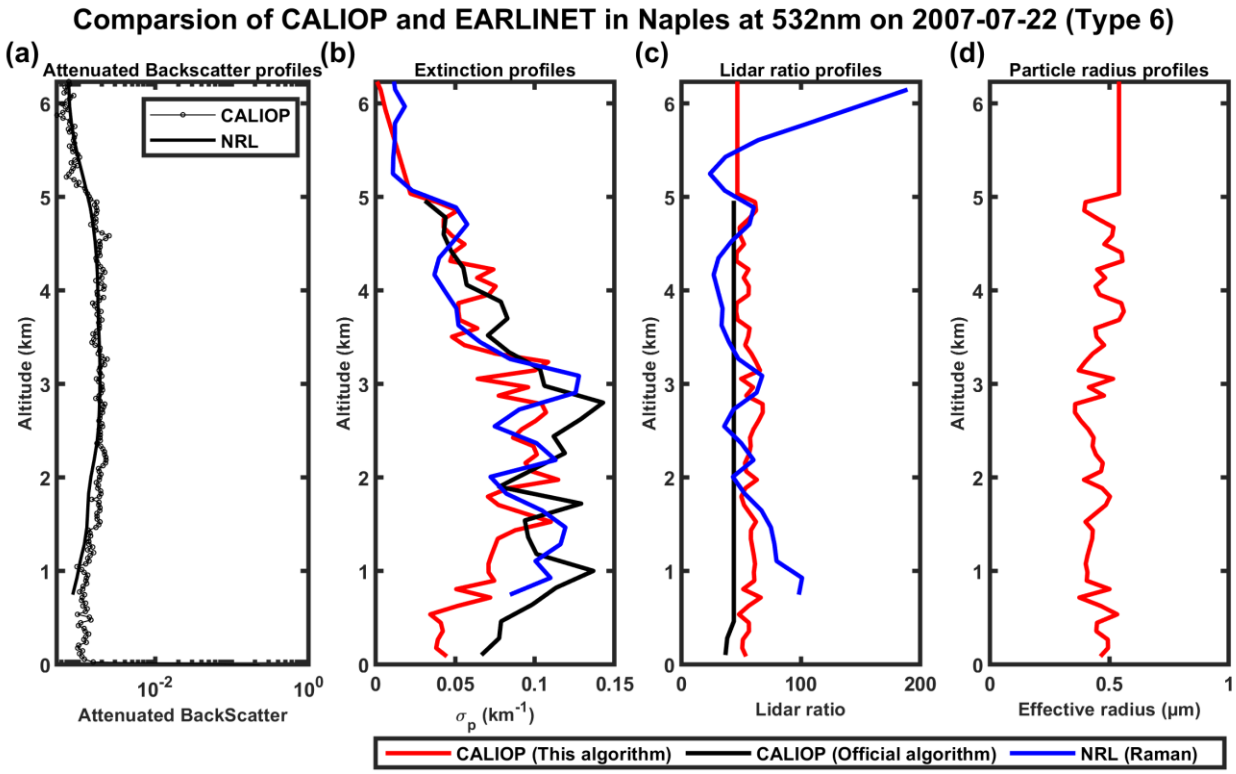

510

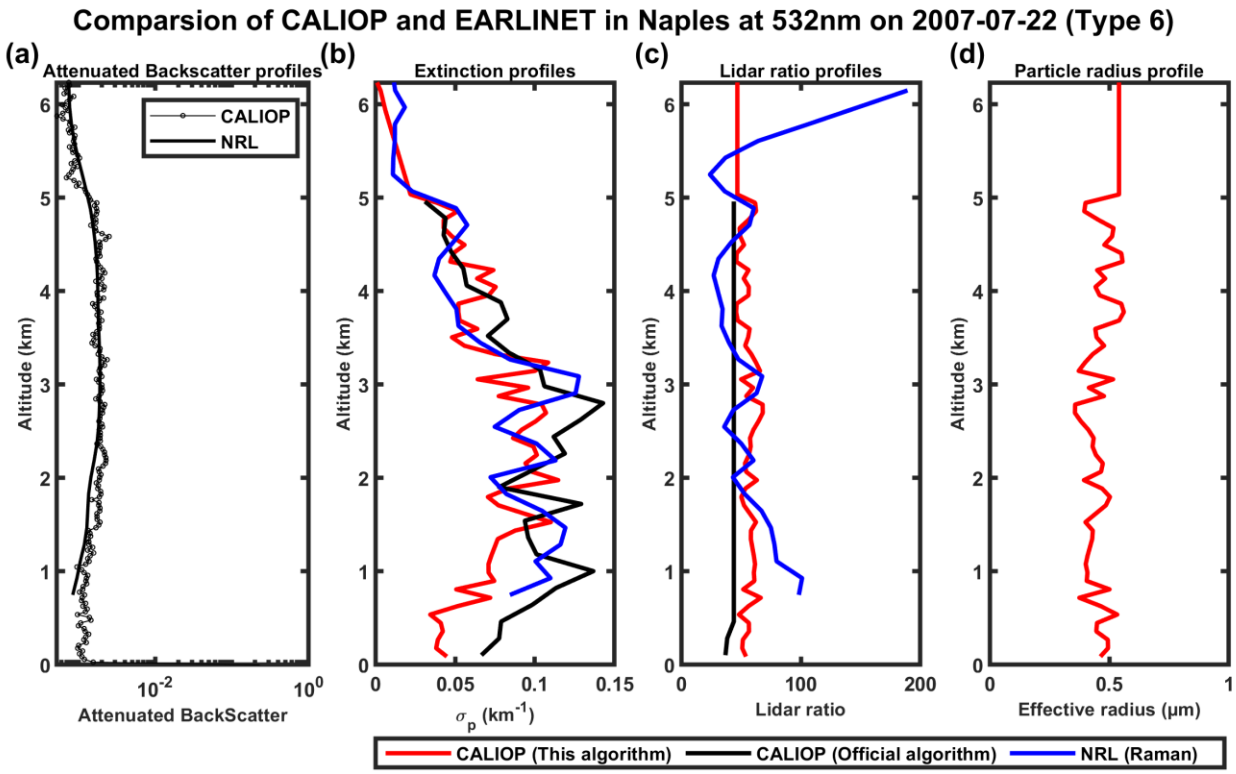

511

512 **Figure 11.** Same as Figure 9 but on 22 July 2007.

513

514

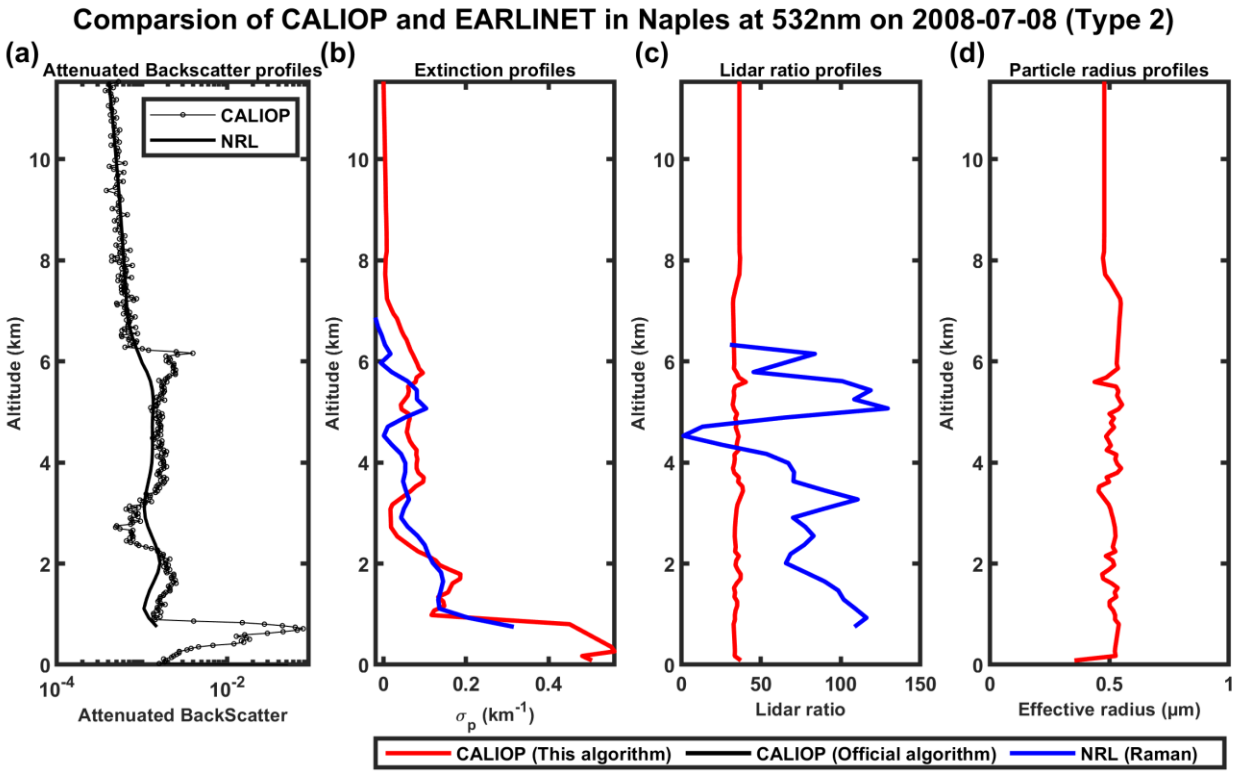

515

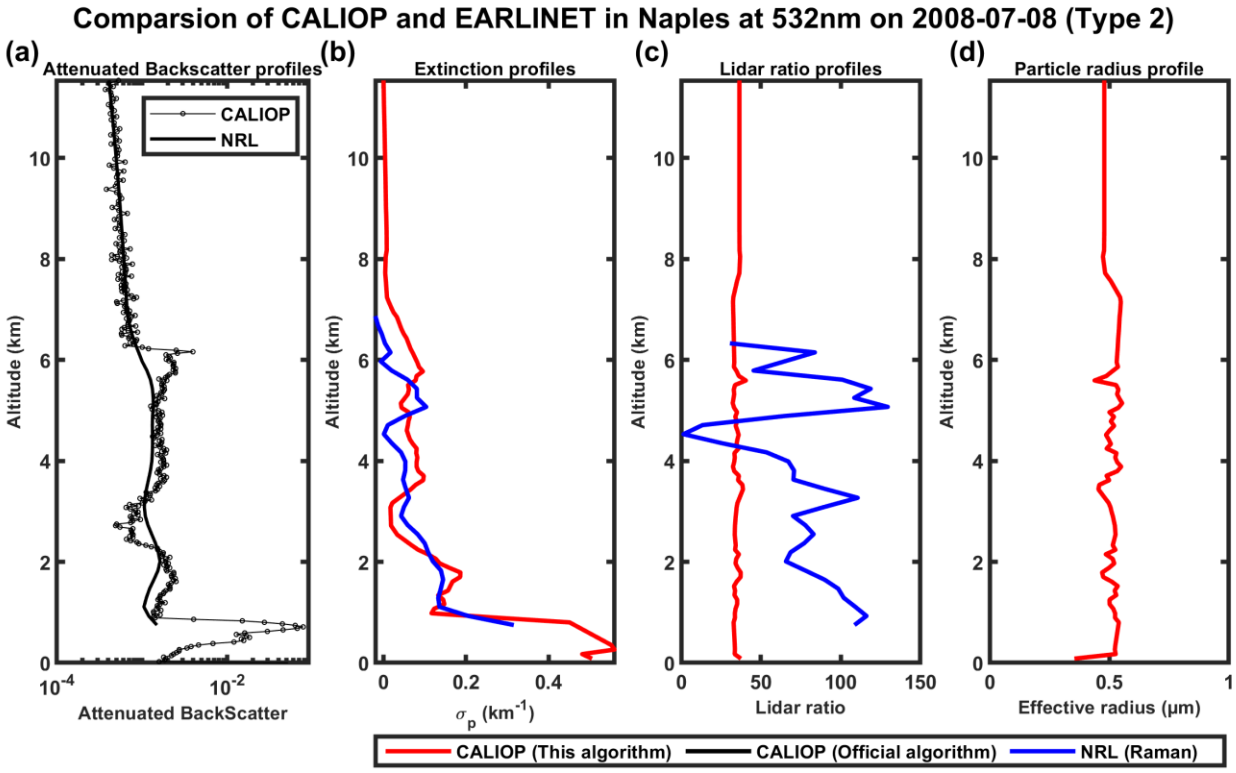

516

517 **Figure 12.** Same as Figure 9 but on 8 July 2008.

518

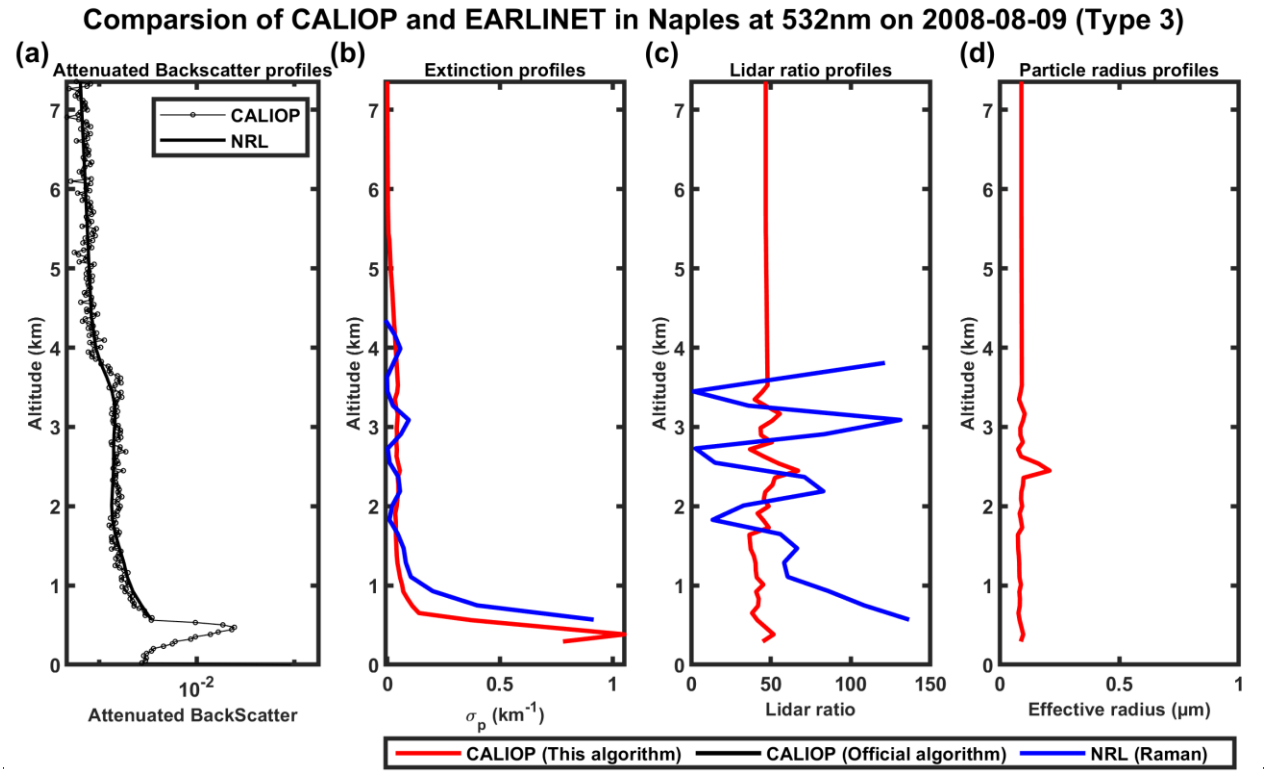

519

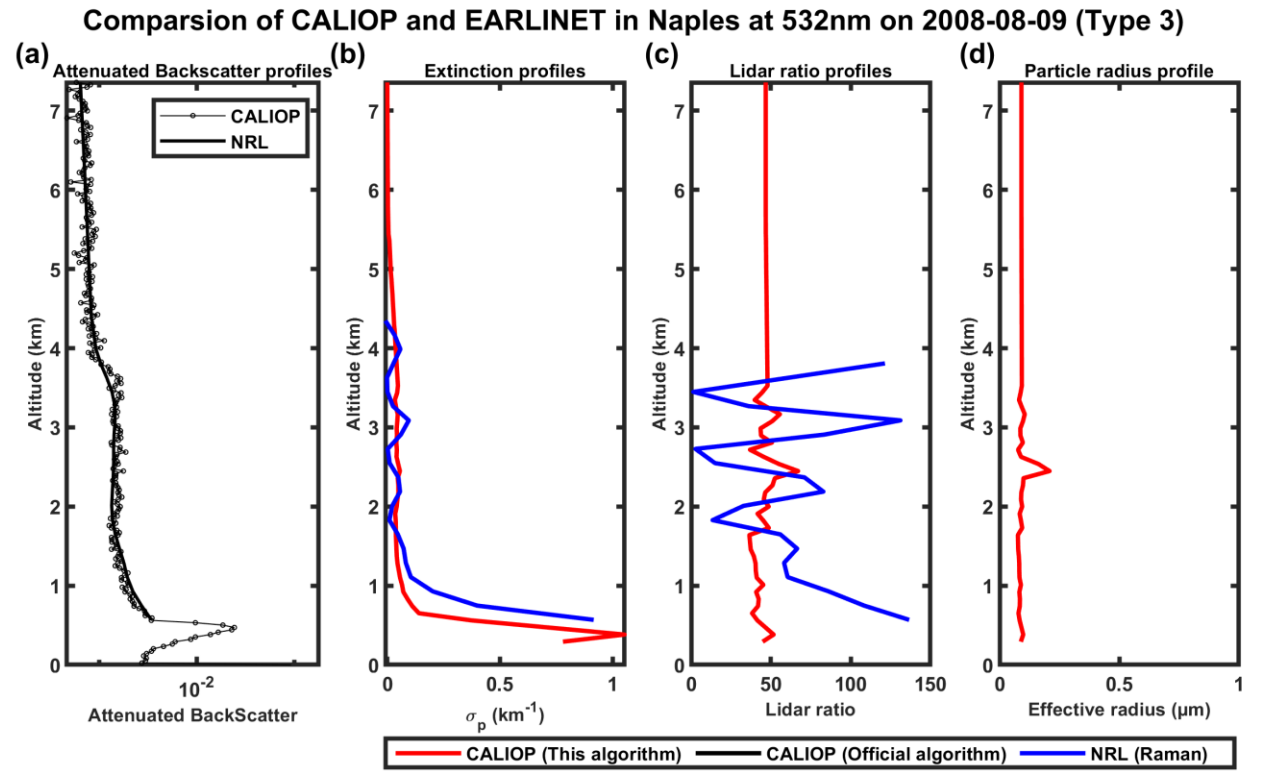

520

521 **Figure 13.** Same as Figure 9 but on 9 August 2008.

522

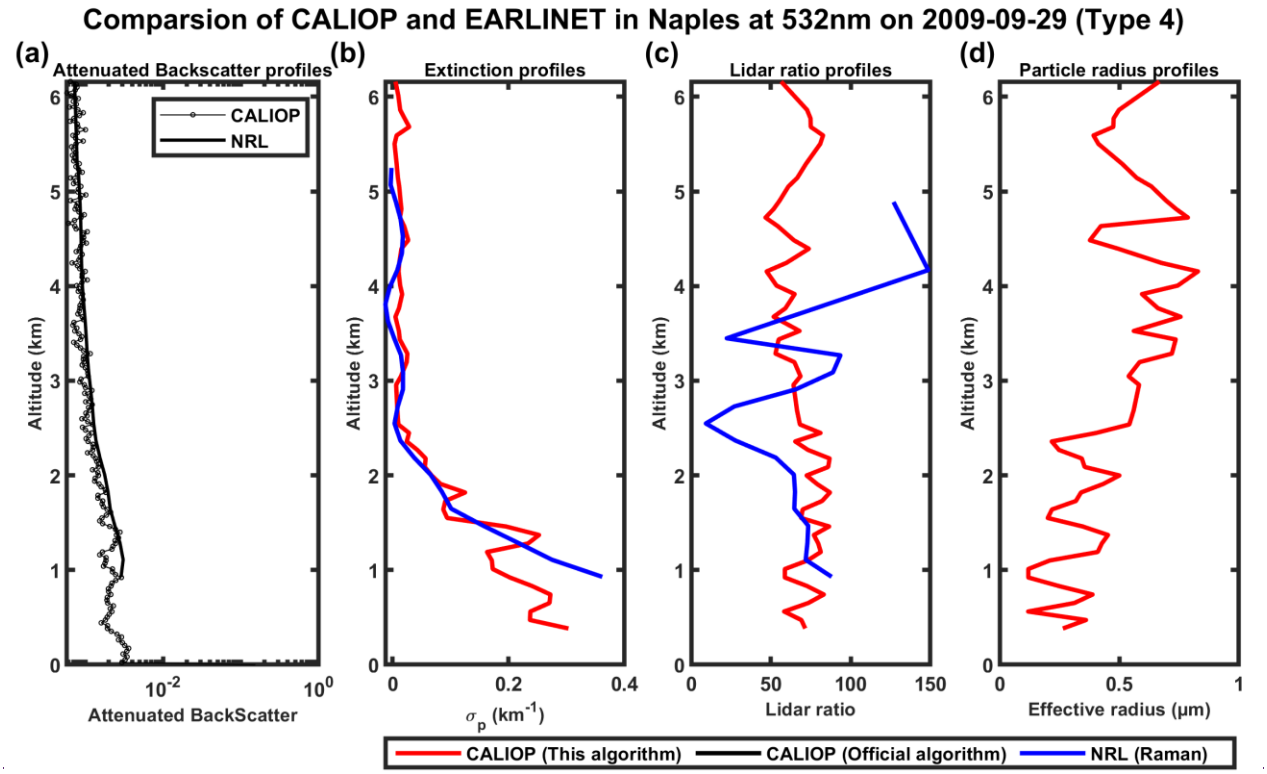

523

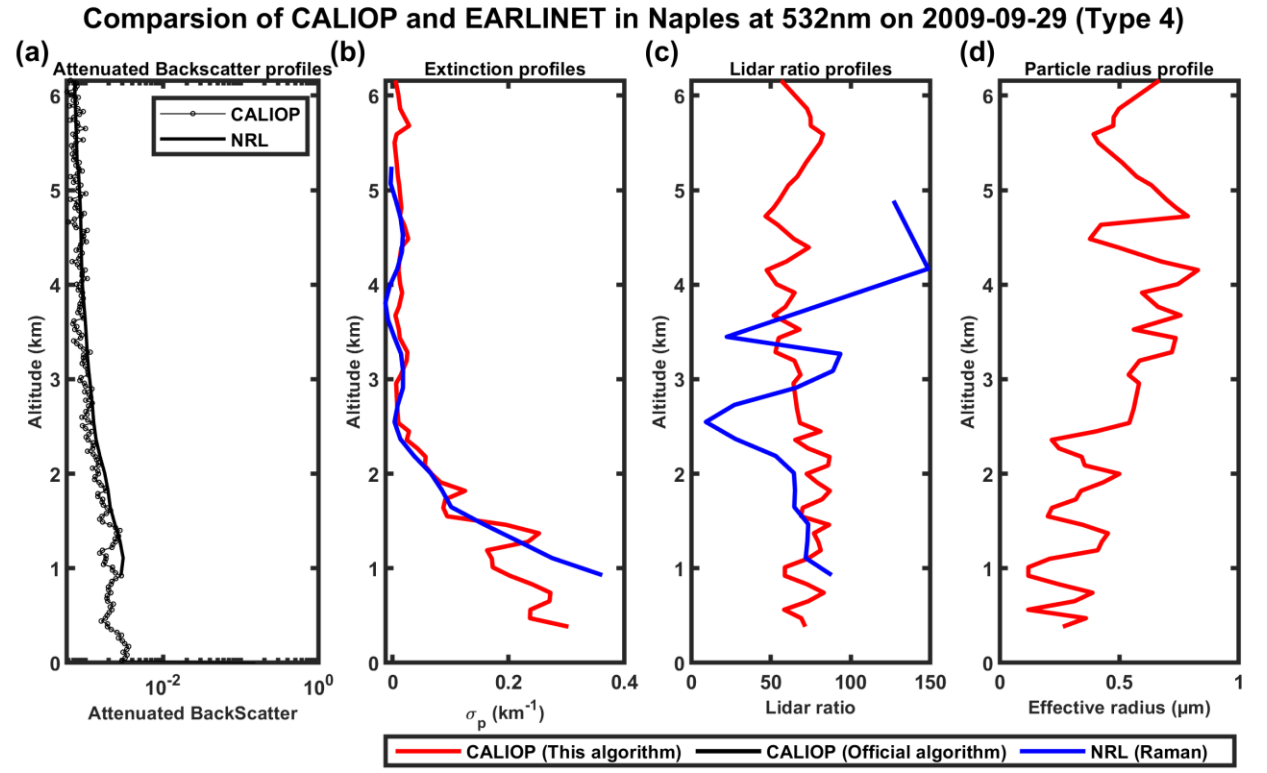

524

525 **Figure 14.** Same as Figure 9 but on 29 September 2009.

526

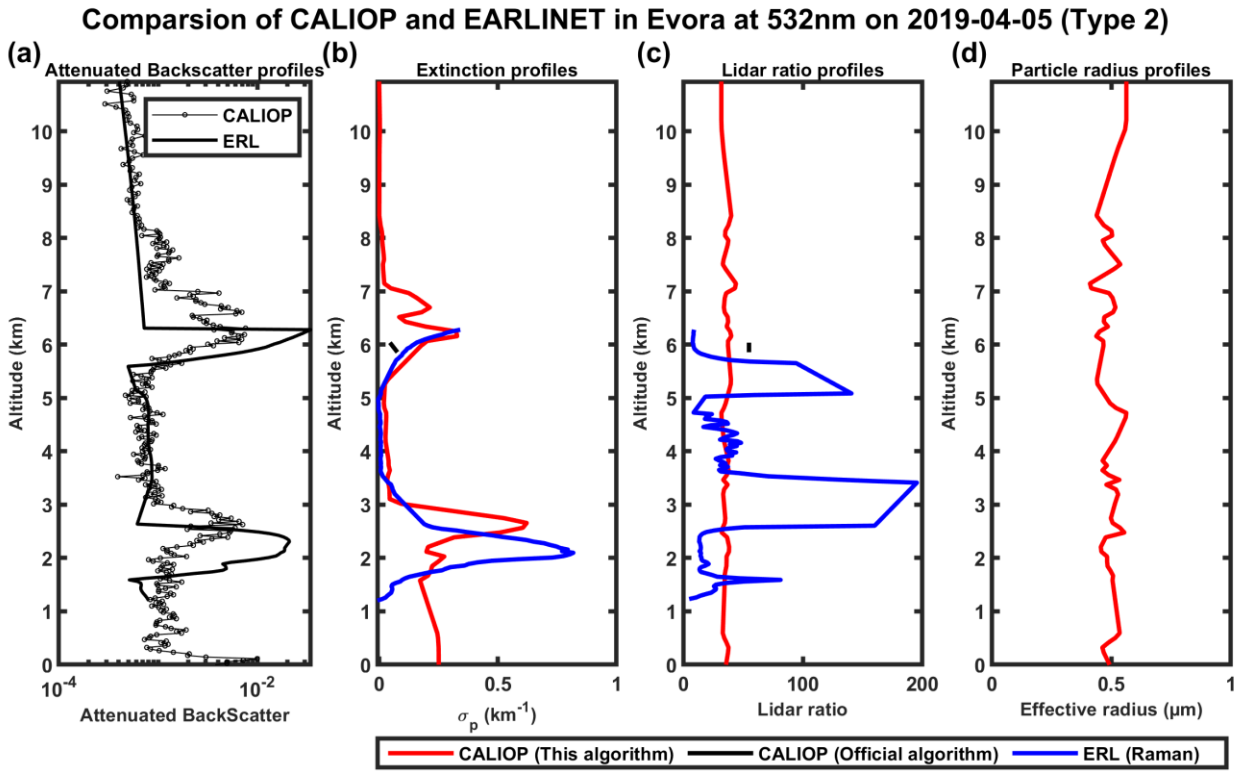

527

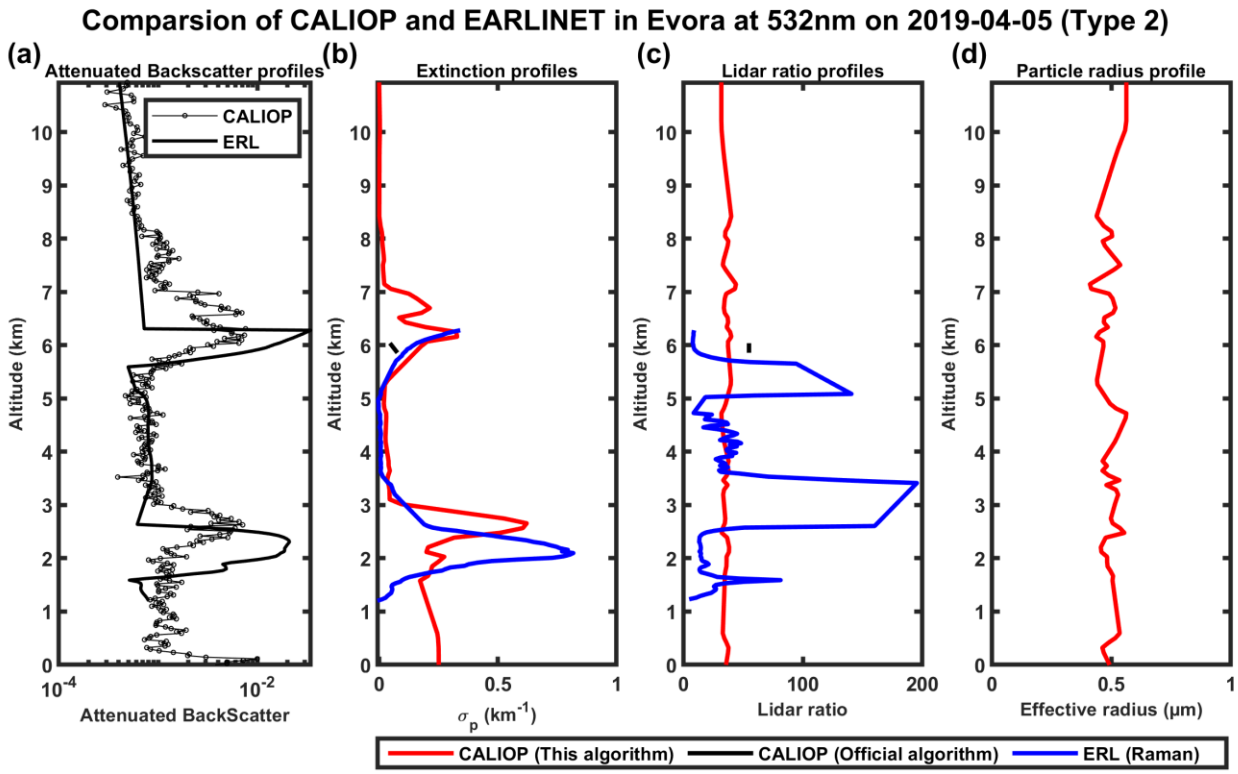

528

529 **Figure 15.** ~~532nm~~532 nm and 106 nm attenuated backscatter profiles measured by CALIOP (black solid line

530 with circle marker) and ERL at the Evora station (remodeling, black solid line) on 20 August 2006 in

logarithmic scale in horizontal direction (a); (b, c, d) show the extinction profiles, lidar ratio profiles and particle radius profiles, respectively, provided by the modified inversion algorithm (red), CALIOP level 2 (black) and EARLINET level 2 (blue).

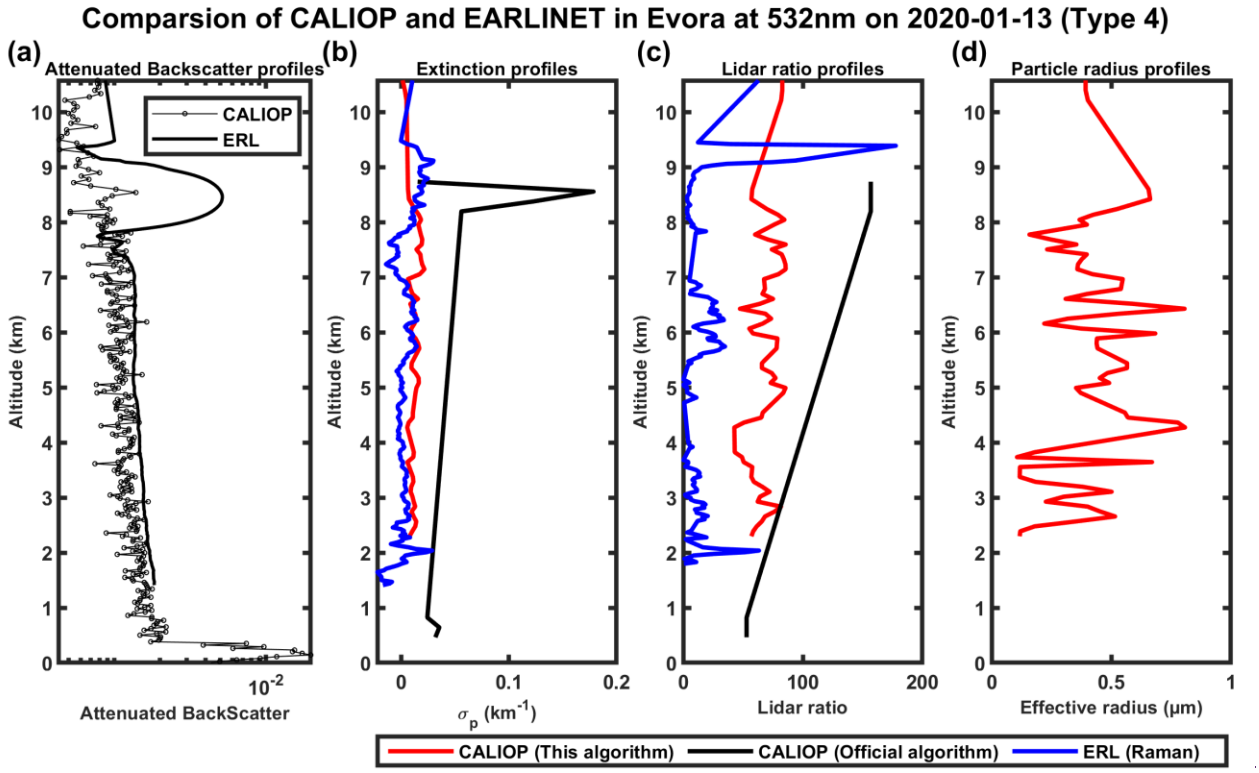

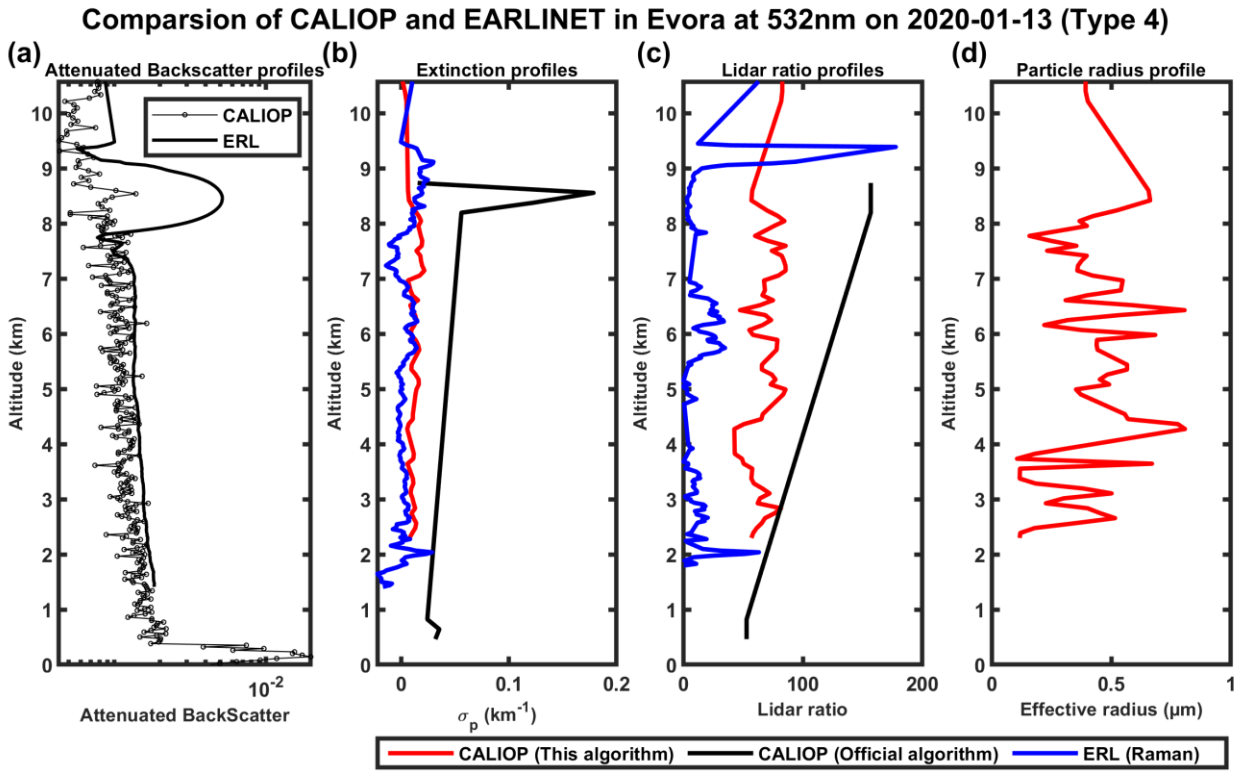

535

536 **Figure 16.** Same as Figure 15 but on 13 January 2020.

537

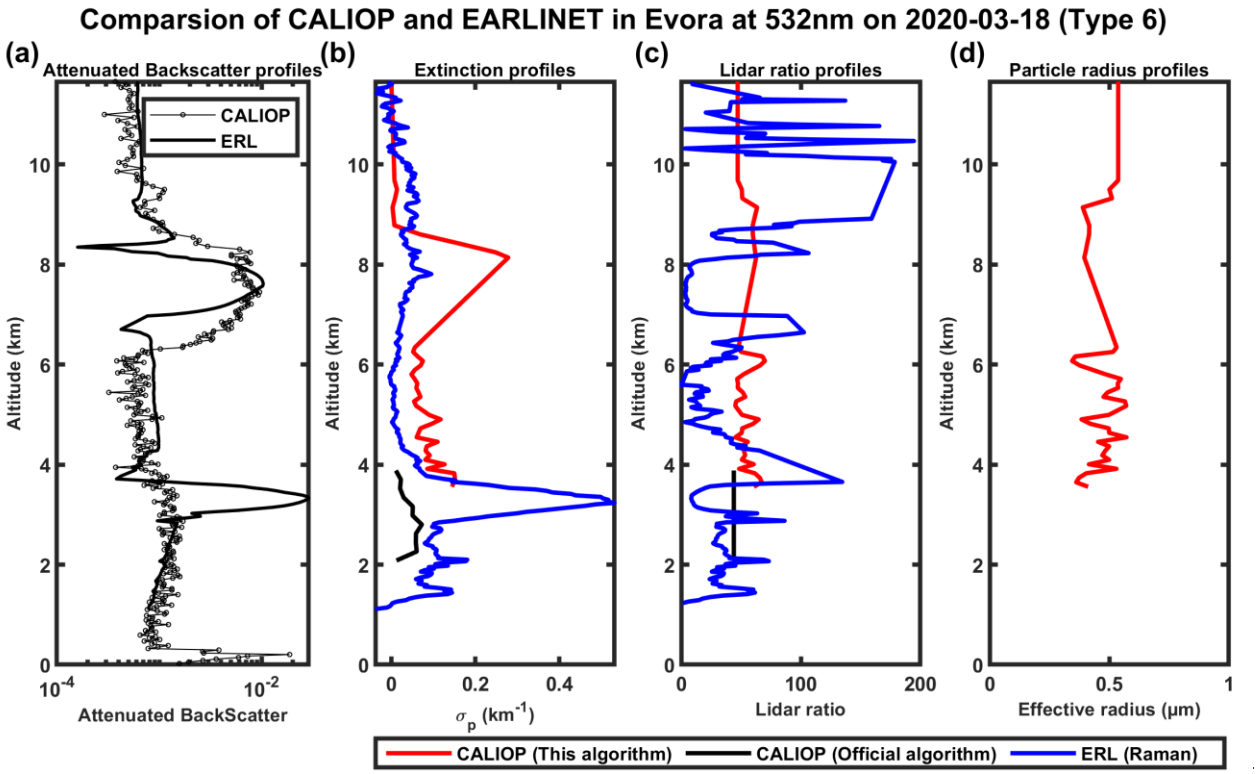

538

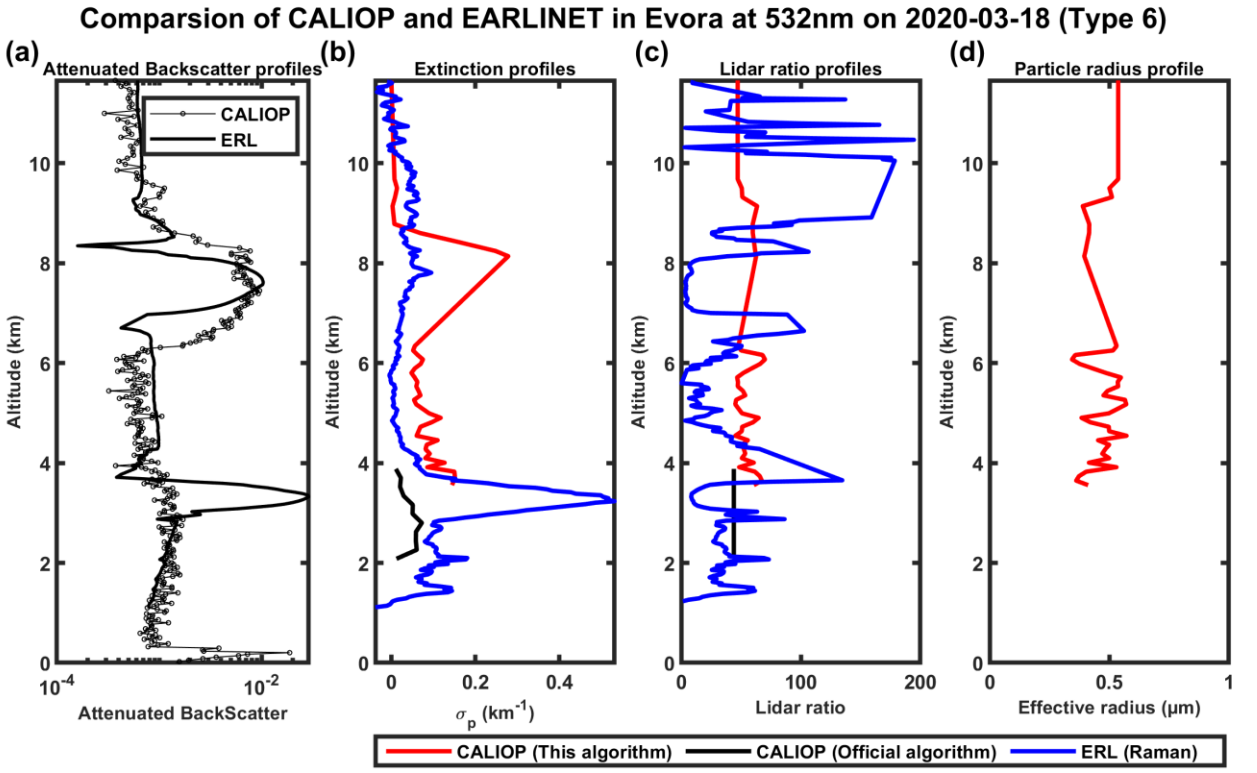

539

540 **Figure 17.** Same as Figure 15 but on 18 March 2020.

541

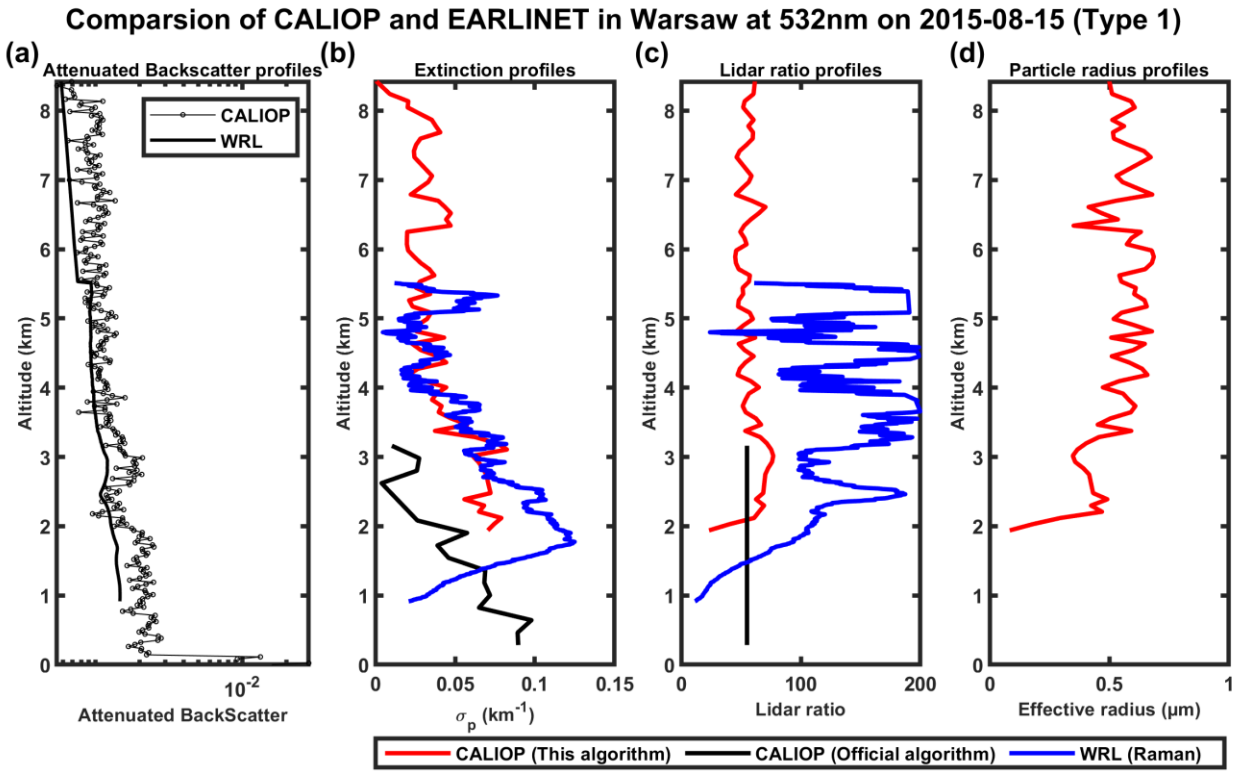

542

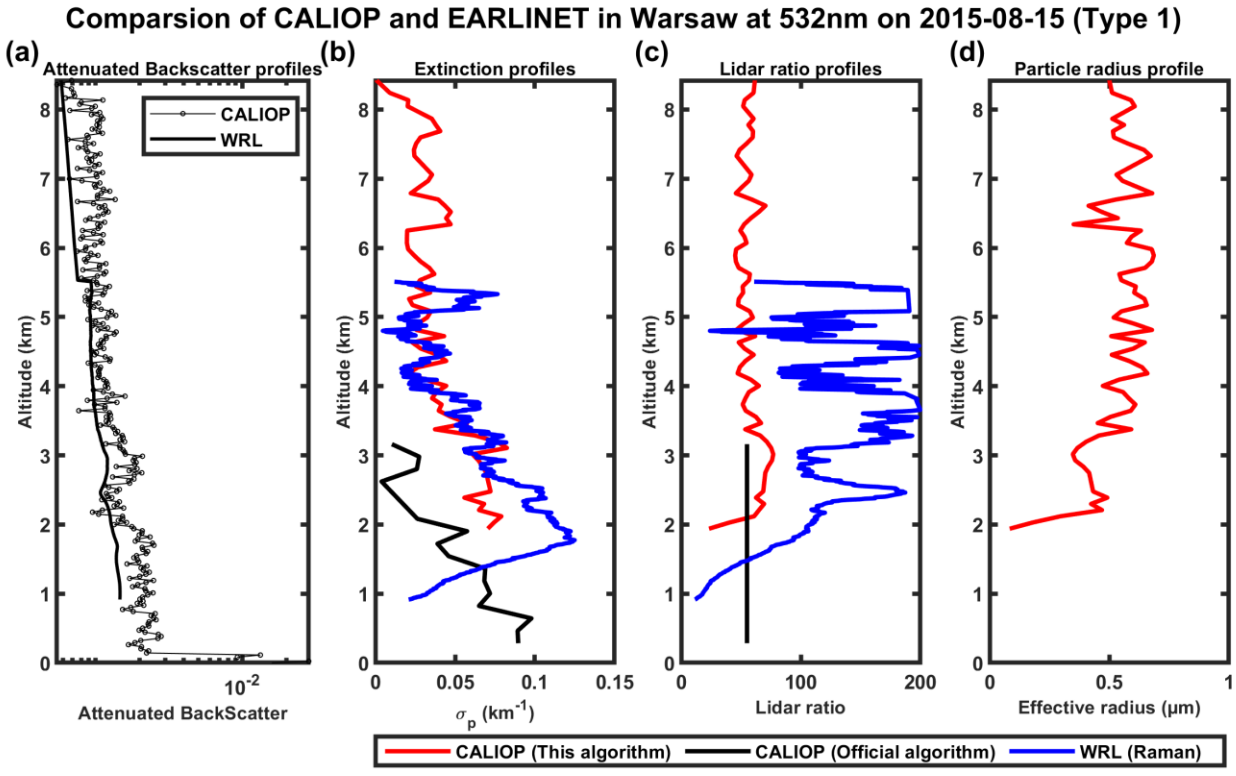

543

544 **Figure 18.** ~~532nm~~532 nm and 106 nm attenuated backscatter profiles measured by CALIOP (black solid line

545 with circle marker) and WRL at the Warsaw station (remodeling, black solid line) on 20 August 2006 in

logarithmic scale in horizontal direction (a); (b, c, d) show the extinction profiles, lidar ratio profiles and particle radius profiles, respectively, provided by the modified inversion algorithm (red), CALIOP level 2 (black) and EARLINET level 2 (blue).

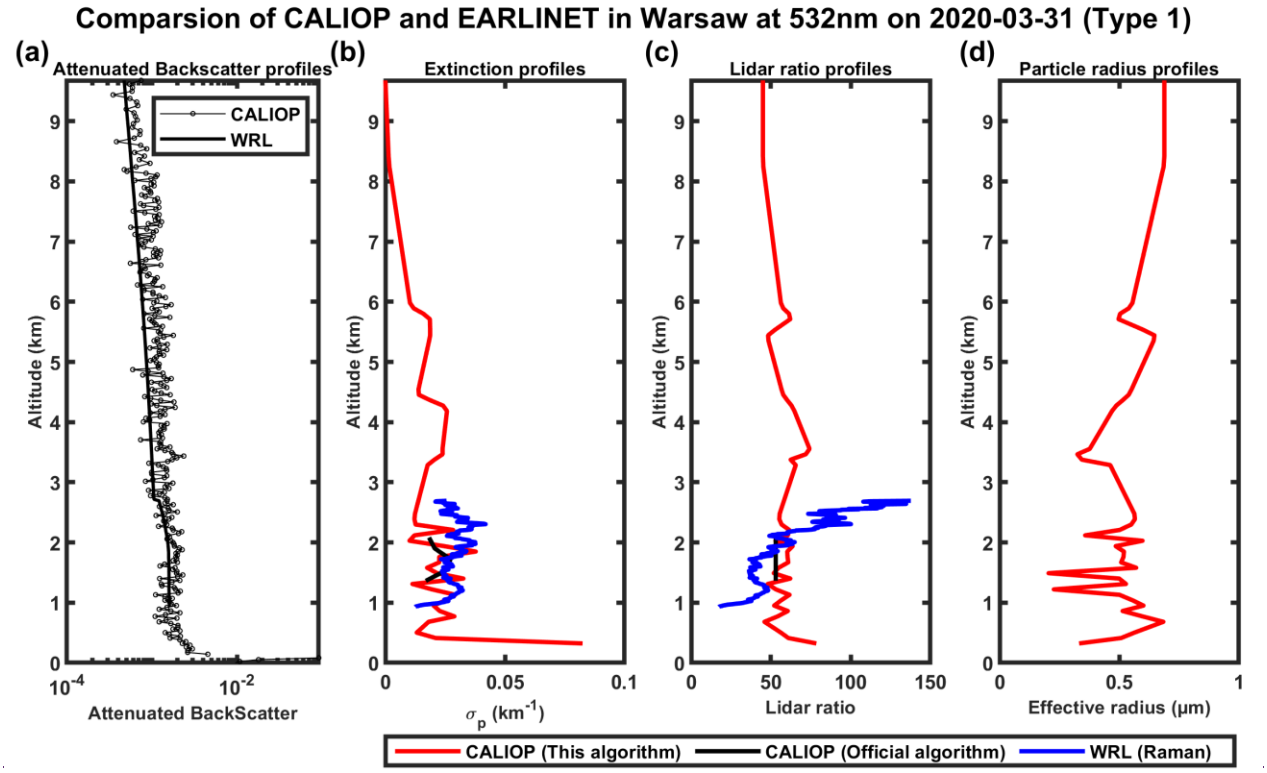

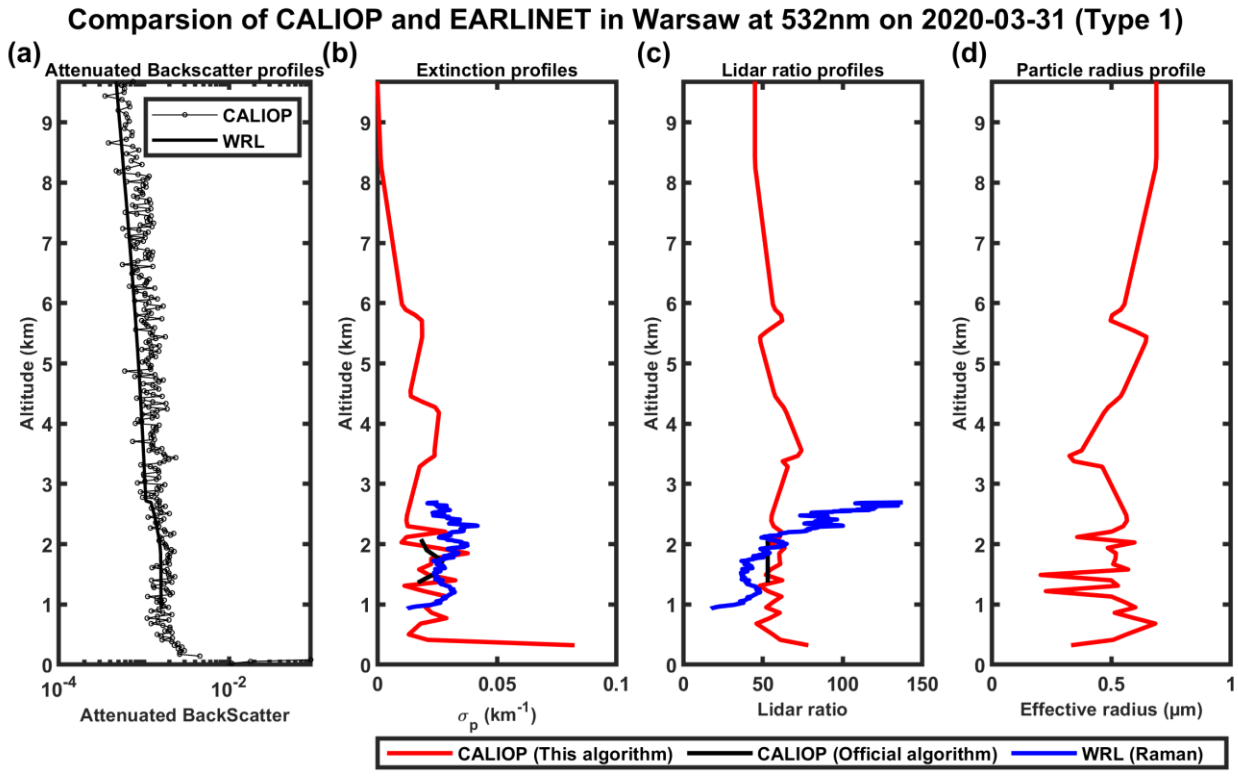

Figure 19. Same as Figure 18 but on 31 March 2020.

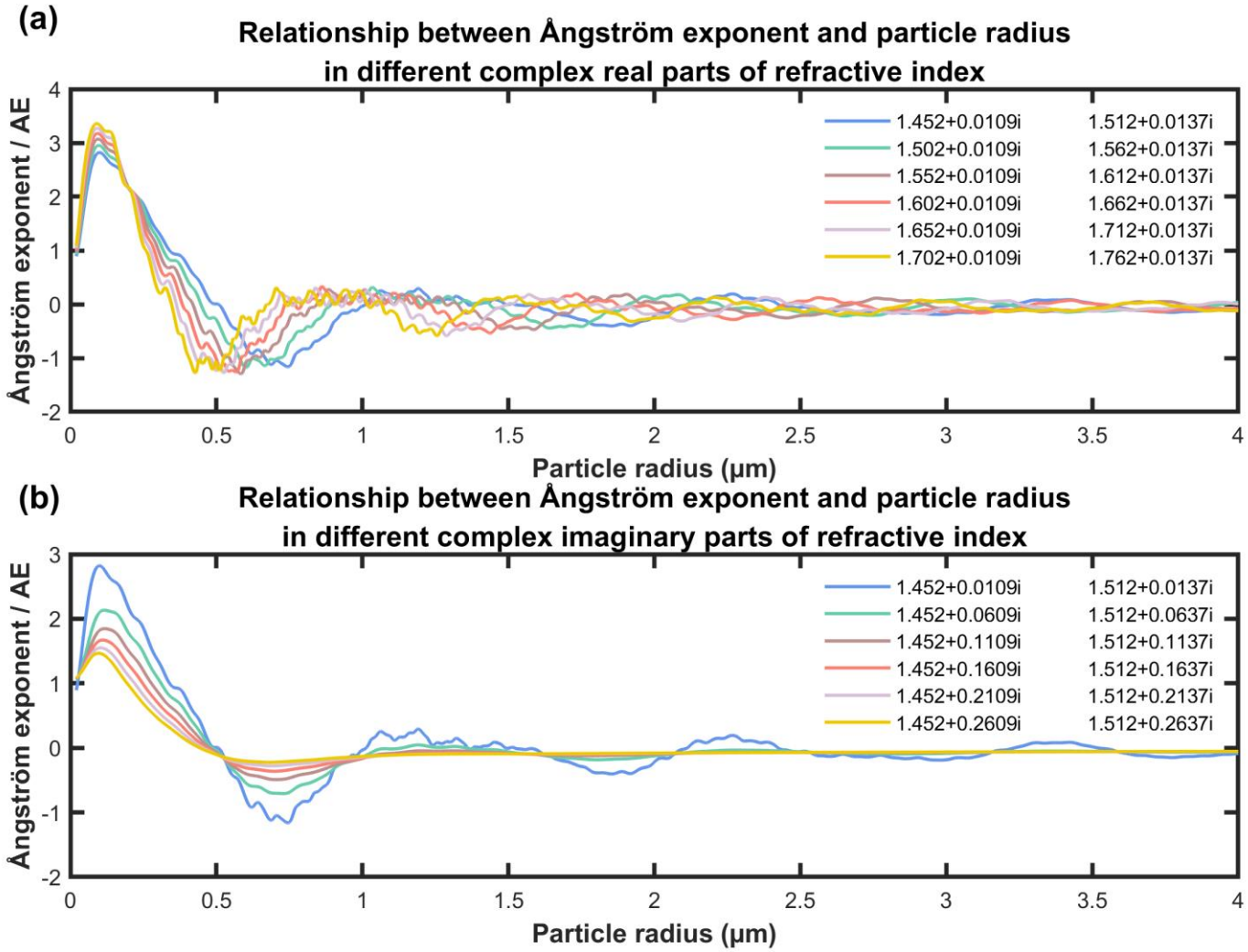

Figure 20. The effect of the complex refractive index on Ångström exponent.